Computational Study of the Cone-Horizontal Cell Feedback Mechanism in the Outer-Plexiform Layer of Cat Retina

by

Shaojie Chang

A Dissertation Presented in Partial Fulfillment
of the Requirements for the Degree
Doctor of Philosophy

Approved April 2012 by the
Graduate Supervisory Committee:

Steven M. Baer, Co-Chair
Carl L. Gardner, Co-Chair
Sharon M. Crook
Yang Kuang
Christian Ringhofer

ARIZONA STATE UNIVERSITY

May 2012

ABSTRACT

In vertebrate outer retina, changes in the membrane potential of horizontal cells affect the calcium influx and glutamate release of cone photoreceptors via a negative feedback. This feedback has a number of important physiological consequences. One is called background-induced flicker enhancement (BIFE) in which the onset of dim background enhances the center flicker response of horizontal cells. The underlying mechanism for the feedback is still unclear but competing hypotheses have been proposed. One is the GABA hypothesis, which states that the feedback is mediated by γ-aminobutyric acid (GABA), an inhibitory neurotransmitter released from horizontal cells. Another is the ephaptic hypothesis, which contends that the feedback is non-GABAergic and is achieved through the modulation of electrical potential in the intersynaptic cleft between cones and horizontal cells. In this study, a continuum spine model of the cone-horizontal cell synaptic circuitry is formulated. This model, a partial differential equation system, incorporates both the GABA and ephaptic feedback mechanisms. Simulation results, in comparison with experiments, indicate that the ephaptic mechanism is necessary in order for the model to capture the major spatial and temporal dynamics of the BIFE effect. In addition, simulations indicate that the GABA mechanism may play some minor modulation role.

ACKNOWLEDGEMENTS

I would like to express my great appreciation to Dr. Steven Baer, for proposing this interesting research project and for his invaluable guidance, support, assistance, encouragements and patience throughout this research.

I feel very grateful to Dr. Carl Gardner and Dr. Christian Ringhofer for their numerous invaluable and detailed instructions and help on programming and numerical methods.

I am equally grateful to Dr. Sharon Crook for her invaluable help on the initial coding of the model and on the various aspects of this research project.

Same gratitude goes to Dr. Yang Kuang for his invaluable time, suggestions and encouragements.

I would like to express my deep thankfulness to Dr. Ralph Nelson, head of Neural Circuits Unit at the National Institutes of Neurological Disorders and Stroke, National Institutes of Health, for his invaluable help in giving important instructions on many biological aspects of this research project, in answering questions on numerous occasions, in recommending useful references, and for his invaluable time and suggestions.

I would like to express my sincere thankfulness to Dr. Maarten Kamermans in the Netherlands Institute for Neuroscience and the Department of Neurogenetics, Academic Medical Center, University of Amsterdam, for his invaluable help in answering many questions related to this project and in providing useful references.

I would also like to thank the School of Mathematical and Statistical Sciences at ASU for supporting my study and research. Special thanks goes to Ms. Debbie Olson for her invaluable assistance over the years.

I would like to thank sincerely my friends David Tello, Jeremiah Jones, Zhun Han, Raquel López, and my other friends in the MathNeuro group and in the

entire School for their great help. Working and studying with them certainly make my stay in the United States more memorable.

Finally, I am indebted to my parents for their longtime support and understanding.

TABLE OF CONTENTS

LIST OF TABLES

LIST OF FIGURES

CHAPTER 1

INTRODUCTION

In this chapter, a brief introduction to the biological background relevant to the research topic is given and then the research objective is stated.

1.1 The outer plexiform layer of mammalian retina

The retina covers the back of the eye where images are formed and light energy is converted into neural signals. Cells in the retina are packed in several layers. The outer plexiform layer (OPL) is the place where photoreceptors make synaptic interactions with bipolar cells and horizontal cells (HCs), and is the first synaptic layer in the visual system. Photoreceptors are light-sensitive cells and can be classified into two major types, rods and cones. Rods are sensitive to very dim light and are responsible for night vision [10]. Vision in bright light depends mainly on cones since they only respond to light of relatively high intensity while the response of rods under such a lighting condition is substantially saturated [10]. Cones also provide the basis for color vision in humans and many other species [10, 146]. In addition, cones respond to light much faster than rods [75]. Consequently, cones can follow flickering stimuli of relatively high frequency whereas rods cannot [26, 93]. Bipolar cells provide the direct pathway for the visual information to flow from photoreceptors to ganglion cells and further into the brain. Horizontal cells receive input from photoreceptors and modulate laterally the responses of adjacent photoreceptors and bipolar cells.

Photoreceptors transduce light energy into graded changes in their membrane potentials. In the dark, photoreceptors depolarize, which opens the voltage-gated calcium channels at the transmitter release sites of photoreceptors' presynaptic axon terminals [10, 84]. Calcium ions thus flow into photoreceptors and the

resulting elevation in the intracellular calcium concentration signals the release of the neurotransmitter glutamate, which then induces the depolarization of postsynaptic horizontal cells and either depolarization or hyperpolarization of postsynaptic bipolar cells depending on the specific bipolar cell types [122, 10, 20, 95]. Light stimulation hyperpolarizes photoreceptors and causes their voltage-gated calcium channels to close. As a result, photoreceptors' intracellular calcium concentration drops and their release of glutamate is suppressed, leading to the hyperpolarization of horizontal cells and the corresponding polarizations of different types of bipolar cells. [122, 10, 59, 95].

The axon terminal of the cone is known as the pedicle. Dendritic terminals (also called spines) of horizontal cells and bipolar cells invaginate into the pedicle to form synapses with the cone at places known as the "triads". A single cone pedicle of humans and primates has about 30 "triads" [1, 18], and one "triad" typically consists of two horizontal cell spines and one bipolar cell spine [60]. Most mammalian retinae have two types of horizontal cells, A-type and B-type [57, 95]. A prominent feature of horizontal cells in all species studied is that cells of the same type are interconnected by numerous electrical synapses known as gap junctions, forming a large conductive sheet or syncytium over a wide spatial area of the OPL [42, 122, 59, 90, 95]. This network organization allows horizontal cells to integrate synaptic inputs from photoreceptors across a large retinal region, and hence increases the receptive-field sizes of individual horizontal cells [95]. The horizontal cells in this study are of A-type, which is axonless and has a dendritic tree with its terminals ending in cone pedicles [59, 95]. Although an A-type horizontal cell does not have direct synaptic contact with rods, it receives rod inputs indirectly from cones since rod signals can enter cones via rod-cone gap junctions [104, 58, 86, 116, 107, 122, 146, 153].

There also exist rod-rod and cone-cone gap-junctional couplings [109, 116, 146, 153]. However, rods are not modeled explicitly here because, as mentioned above, the A-type horizontal cells considered in this study only interact directly with cones. Therefore, as the next chapter will show, rod signal is expressed as a direct current input in the equation for cones. Furthermore, the coupling among cones is not as strong and extensive as that among horizontal cells [70, 24], so this feature is omitted to simplify the model.

1.2 The background-induced flicker enhancement effect

In cat retina, the onset of diffusive rod-selective dim blue background amplifies the response amplitudes of the membrane potentials of horizontal cells at the center of the retina region stimulated by small-spot cone-selective photopic red flicker [98, 88]. This phenomenon is called the background-induced flicker enhancement (BIFE) effect [98, 88]. To quantify the enhancement, a variable E named "percent enhancement" was defined by

$$E = 100(F_{bkgd}/F_{dark} - 1) \tag{1.1}$$

where F_{bkgd} and F_{dark} are the mean response amplitudes of horizontal cells during background illumination and dark, respectively [34]. Intracellular staining demonstrated that the horizontal cells involved in the BIFE effect are mainly of A-type [98].

There are some characteristic temporal and spatial features associated with the BIFE effect, four of which will be examined carefully in this study. First, the membrane potentials of horizontal cells repolarize slowly (the "sag") during the hyperpolarized stage in the presence of background, and then generate an "overshoot" or post-inhibitory rebound (PIR) through slow depolarization once the background is turned off [98]. Second, the curve of E as a function of flicker frequency re-

veals a two-limbed nature with E increasing gradually below around 20 Hz and rising up rapidly above this frequency [98]. Third, a phase advance of the flicker waveform is induced by the background. That is, the averaged waveform of one oscillation period of the horizontal cell membrane potential occurs 2$\sim$5 ms sooner with background on than that with background off [98]. Finally, for both slit and square regions of flicker stimulus, E decreases monotonically as the size of the flicker stimulus region increases [88].

It is worth mentioning that the BIFE effect is closely analogous to the "suppressive rod-cone interaction" (SRCI) observed in human psychophysics, animal electrophysiology, and human and animal electroretinograms (ERGs) [37, 33, 2, 32, 43]. SRCI is the common phenomenon that cone-mediated sensitivity to small-spot flicker stimuli, especially those of high frequencies, is suppressed when rods are dark-adapted and is enhanced by rod-selective backgrounds [37, 33].

1.3 Hypotheses on cone-horizontal cell feedback mechanism

In addition to the feedforward synaptic transmission from cones to horizontal cells using glutamate as the neurotransmitter, there exists a negative feedback from horizontal cells to cones: hyperpolarized horizontal-cell dendritic terminals somehow increase the flow of calcium ions into cone pedicle, stimulating glutamate release by the cone presynaptic apparatus and leading to depolarized responses of horizontal-cell dendritic terminals [36, 52, 49, 48, 44, 95]. This feedback mediates color opponency in second-order retinal neurons [53, 121, 146] and plays an important role in the formation of center-surround receptive field organizations of bipolar cells and ganglion cells [10, 52, 87, 95, 139, 142, 146]. It is also generally accepted that the BIFE effect can be accounted for by this feedback: a dim full-field background illumination induces a rod-mediated strong hyperpolarization of horizontal cells across their syncytium, and this hyperpolarization gives rise to, through the feedback, an

augmented calcium entry into cone pedicles; the increase in calcium current is usually linked to enhanced amplitude modulations of the current itself and of the released transmitter glutamate, which then results in enlarged response amplitudes of the postsynaptic horizontal cells [88, 52, 131]. For a schematic illustration of how the cone-horizontal cell feedback might bring on flicker enhancement, please refer to Figure 5 in paper [131].

It remains unclear about the underlying mechanism that relates the hyperpolarization of horizontal cells to the rise of calcium current into cone pedicles during the feedback, and three competing hypotheses were proposed to address this question, namely, the GABA, ephaptic, and pH hypotheses.

The GABA hypothesis

By and large, the GABA hypothesis conceives that γ-aminobutyric acid (GABA) acts as the inhibitory neurotransmitter from horizontal cells to cones. One version of the GABA hypothesis states that depolarized horizontal-cell dendritic terminals in darkness release a substance which blocks the calcium channels on the cone pedicles, with the major candidate for such a substance being GABA; background-induced hyperpolarization of horizontal cells inhibits their release of GABA, allowing more calcium ions to enter the cone synaptic terminals [29, 36, 88, 100]. In addition, this version also proposes that the enhanced entry of calcium ions during background illumination opens calcium-activated chloride channels on the cone pedicle [88]. Figure 9 of paper [88] illustrates the biological model described above. A second version of the GABA hypothesis assumes that GABA released by depolarized horizontal cells slightly hyperpolarizes cones by eliciting, via GABA receptors, a chloride current into cones, and a diminished release of GABA accompanying horizontal-cell hyperpolarization shuts down the chloride channels and hence

depolarizes the cones [13, 16, 54, 87, 145, 146]. It's natural to expect that this depolarizing cone response would then increase cone calcium influx [52].

The GABA hypothesis has some experimental support. First, many animal species including mammals have one or more types of horizontal cells which contain GABA and express the GABA-synthesizing enzyme glutamic acid decarboxylase (GAD) [19, 38, 47, 67, 77, 105, 112, 132]. Second, horizontal cells release GABA upon depolarization [3, 78, 110, 111, 150]. Third, GABA decreases the calcium conductance in some sensory neurons [22, 27, 28, 29]. Fourth, GABA receptors and associated chloride currents were shown to exist at some nonmammalian and mammalian cone axon terminals [54, 124, 99, 92, 133, 151]. Finally, GABA antagonists used in several pharmacological studies alter the light responses of certain types of cones and horizontal cells, indicating GABA as the feedback neurotransmitter from horizontal cells to cones [66, 82, 83, 129, 145].

However, there are arguments against the GABA hypothesis. For example, an experimental investigation on turtle cones concludes that the GABAergic system may be too weak to generate the cone-horizontal cell feedback response under physiological conditions [125]. Moreover, some experiments demonstrate that feedback responses of cones evoked by surround illuminations are unaffected by GABA antagonists [41, 125, 126, 135] or GABA agonists [126]. Thirdly, it is still controversial whether monkey and human retinal horizontal cells contain GABA [61]. In addition, nonmammalian retinae have two to five types of horizontal cells but usually only one type accumulates and synthesizes GABA, so the other types of horizontal cells in these species must use non-GABAergic transmitter(s) or mechanism(s) for synaptic feedback [67, 112, 124].

In this study, we focus our attention on the first version of the GABA hypothesis for the following reasons. First, GABA and several other related chemi-

cals were shown to have a direct effect on the inward calcium current [9, 22, 27, 29, 40, 79]. Second, the involvement of chloride ions in negative feedback is most likely to be secondary to the calcium influx since cones have calcium-activated chloride currents [7, 14, 52, 62, 80, 88, 100, 127, 135, 134, 147]. Third, most experiments showed that surround illumination increases both the calcium conductance and chloride conductance of the cone membrane [36, 52, 69, 91, 135, 134], which is consistent with the first version of the GABA hypothesis.

The ephaptic hypothesis

The ephaptic hypothesis contends that the feedback from horizontal cells to cones is non-GABAergic and is achieved through modulation of the electric potential in the intersynaptic cleft between cones and horizontal cells. The hypothesis was initially proposed by Byzov and colleagues [15], and was later modified by Kamermans and colleagues who postulate that hemichannels (half of a gap junction) on the dendritic tips of horizontal cells form the major current sink necessary for an ephaptic mechanism [49, 48]. The hypothesis speculates that in the dark there is a small inward current going from extracellular space into horizontal cell dendritic tips through the intersynaptic cleft and hemichannels, and this current creates a voltage drop over the relatively high resistance of the cleft, making the potential deep in the cleft slightly negative. Light-evoked hyperpolarization of horizontal cells leads to an increase of this hemichannel-mediated current, which results in a larger voltage drop over the intersynaptic resistance and thus a more negative potential in the cleft. Consequently, the nearby voltage-gated calcium channels on the presynaptic membrane of the cone pedicle sense a local cross-membrane depolarization and hence are more prone to open, boosting the calcium influx. In voltage-clamp recordings of cones, this feedback-induced increase of calcium current is observed as a shift of

the cone calcium current-voltage relationship toward more negative potentials. A schematic diagram of the ephaptic feedback mechanism is depicted in Figure 3 in paper [48].

The ephaptic hypothesis is buttressed by a number of findings. First, in goldfish, it was found that horizontal cell hyperpolarization evoked by surround illumination shifts the cone calcium current activation range to more negative potentials in a GABA-independent manner [135]. Second, feedback-mediated responses in cones and horizontal cells can be greatly reduced or eliminated by gap junction blockers such as carbenoxolone [49, 101, 134] and a low concentration of Co^{2+} [30]. Third, immunoreactivity to connexins, the hemichannel-forming proteins, were confirmed to exist on horizontal-cell dendritic tips inside the cone pedicles of carp and zebrafish retinae [46, 49, 114]. Furthermore, feedback responses in cones and horizontal cells are impaired in mutant zebrafish lacking connexin hemichannels which are specific to horizontal cells [44]. In addition, a few ephaptic-hypothesis-based model simulations of the cone-horizontal cell synapse are in line with the experimental investigations of the feedback [30, 31, 44].

The ephaptic hypothesis has some problems, too. For instance, a computational analysis indicates that an effective electrical feedback would require an improbably large intersynaptic resistance and physiological restrictions limit this resistance to values at which the electrical feedback signal generated by horizontal cell hyperpolarization would be negligible [25]. Doubts were also raised over the pharmacological specificity of carbenoxolone since the drug not only blocks hemichannels but also has direct and strong inhibitory effect on photoreceptors' voltage-gated calcium channels [25, 137, 134]. Hemichannels might produce additional issues since they could be the leakage sites through which small molecules (including neurotransmitters such as GABA) inside the horizontal cell can enter

the intersynaptic cleft [112]. There are other concerns on the feasibility of a hemichannel-mediated ephaptic mechanism; please refer to papers [25, 112, 117] for details.

The pH hypothesis

The pH hypothesis provides an alternative non-GABAergic feedback mechanism: extracellular pH changes in the intersynaptic cleft mediate the feedback [8, 41]. Specifically, it proposes that horizontal cell hyperpolarization alkalinizes the cleft, and the decrease in extracellular proton concentration then alters the gating of pH-sensitive calcium channels in the presynaptic cone pedicle and results in an increase of cone calcium current in the form of a negative shift of the current's activation potential [8, 41]. The mechanism by which horizontal cell polarization modulates the extracellular pH is still unknown, although hemichannel-mediated proton transport [48], amiloride-sensitive proton channels [138], or some other proton transport system [12, 41] on the horizontal cell dendritic tips might be possible candidates.

There are experimental studies supporting the pH hypothesis. First, protons were shown to have inhibitory effects on voltage-gated calcium channels [23, 102]. Second, there are experiments reporting that light stimulation induces extracellular alkalinization in distal retina around photoreceptors [89, 148]. Third, the voltage dependence of photoreceptor calcium channels were indeed shifted to more negative potentials upon extracellular alkalinization [6, 8, 41], and it was estimated that an increase of extracellular pH by 0.1 units shifts the calcium channel activation range negatively by about 1.2$\sim$1.67 mV for tiger salamander photoreceptors [6, 8]. Finally, prevention of extracellular pH fluctuations with a high concentration of HEPES and some other artificial pH buffers abolishes or substantially attenuates the feedback responses in both cones and horizontal cells in the retinae of goldfish, newt, tiger salamander and macaque monkey [4, 16, 21, 41, 138], and the reduction

of feedback is positively correlated to elevation of the pH buffering capacity of the bath solution [21].

The legitimacy of the pH hypothesis has also been questioned. One experimental finding demonstrates that glutamate, the neurotransmitter known to depolarize horizontal cells, induces a decrease of proton concentration in the extracellular fluid near the membrane of catfish cone- and rod-driven horizontal cells, which is precisely contrary to the prediction made by the pH hypothesis [65]. In some other experiments on carp and goldfish, the feedback responses of both cones and horizontal cells remain normal in the presence of high concentrations of HEPES [76, 48]. More importantly, it was suggested that, in addition to clamping the extracellular pH, artificial pH buffers induce horizontal-cell intracellular acidification which is known to inhibit hemichannels [31, 117]; therefore the above-mentioned pH buffer experiments supporting the pH hypothesis may fail to distinguish between a pH-mediated and a hemichannel-mediated feedback mechanism [31].

1.4 Research objective

The aim of the present study is not to give a mathematical explanation of the BIFE effect, but to use the BIFE effect as a vehicle to conduct a computational examination of the feedback mechanism between cones and horizontal cells in cat retina. A partial differential equation (PDE) model incorporating both the GABA and ephaptic hypotheses will be developed. This study does not pay particular attention to the pH hypothesis because experimental investigations showed that protons can inhibit calcium channels by both reducing channel conductance directly [17, 102] and by shifting channel activation to more positive potentials [55, 64]. Thus the pH mechanism, if it works, may resemble a combined effects of the GABA and ephaptic mechanisms, and incorporating it into the model will complicate the analysis. The PDE model will be solved by finite difference methods, and simulation results of

the model will be compared with experimental data in cat retina under different spatial and temporal settings. Hopefully, this study provides insights into which mechanism, GABA or ephaptic, might be more appropriate.

CHAPTER 2

THE MATHEMATICAL MODEL

In this chapter, a reaction-diffusion system of partial differential equations is formulated to model the interaction between cones and horizontal cells in a patch of retina on the xy-plane. The model is a generalization of a continuum spine formulation developed for dendritic cables with spines [5]. The horizontal cell slab is treated as a two-dimensional continuum with continuously distributed spines forming synapses with cone pedicles. The model incorporates both GABA and ephaptic feedback mechanisms and captures dynamics on two spatial scales: the scale of an individual synapse and the scale of the receptive field. By default, all state variables are functions of the spatial variables x and y and the time variable t, and all membrane potentials involved are cross-membrane potential differences (i.e., intracellular potential minus extracellular potential). The model follows the convention in neuroscience with an outward current having a positive sign and an inward current having a negative sign [56].

2.1 The horizontal cells

The membrane potential V_H (mV) in the horizontal cell slab is governed by a current balance equation involving the capacitive, gap-junctional, stem, and ionic currents:

$$C_m \partial_t V_H = \frac{1}{R_s} \nabla^2 V_H + \overline{N} I_{ss} - I_{ion} \tag{2.1}$$

where

$$I_{ss} = \frac{U_H - V_H}{R_{ss}} \tag{2.2}$$

is the point current at (x,y) flowing between an individual spine head with membrane potential U_H (mV) and the horizontal cell slab through a spine stem with lumped Ohmic resistance R_{ss} (MΩ), and $\overline{N}$ is the physical spine density defined

as the number of spines per unit physical area [5]. C_m (μF/cm^2) is the specific membrane capacitance. The Laplacian term $\frac{1}{R_s}\nabla^2 V_H$ accounts for the density of the current flowing through the gap-junction-coupled slab of horizontal cells with R_s (MΩ) being the sheet resistance [85, 68]. I_{ion} (μA/cm^2) is the density of the ionic currents passing through horizontal cell membrane and its expression will be given later in Eqs. (2.7) $\sim$ (2.10).

The spine stem resistance is defined as $R_{ss} = (4LR_i)/(\pi d^2)$ with the spine stem being treated as a circular cylinder of diameter d, length L and constant intracellular resistivity R_i [113]. In cat, R_i is about 200 $\Omega \cdot$ cm [56, 115] , d is about 0.1 μm, and L is as long as or longer than 5 μm. For these values, R_{ss} is around 1300 MΩ, which is within the estimated range of $10^7 \sim 10^{10}$ Ω for R_{ss} [113].

In this study, the model assumes a uniform spine distribution. A typical mammalian cone pedicle makes synaptic contacts with about 60 horizontal cell spines because one cone pedicle is associated with approximately 30 "triads" of invaginated processes of second-order neurons [1] and each "triad" usually contains two horizontal cell dendritic terminals [60]. A modest estimate of cone density for cat retina is roughly 6.4×10^5 cones/cm^2 [120, 143]. Multiplying the number of spines per cone pedicle with the cone density yields a physical spine density of $\overline{N} = 3.84 \times 10^7$ spines/cm^2 for cat.

Multiplying both sides of Eq. (2.3) by the passive membrane resistivity R_m ($\Omega \cdot$ cm^2), and substituting the known relations for the membrane time constant $\tau_m = R_m C_m$ [56], the horizontal-cell slab length constant $\lambda = \sqrt{R_m/R_s}$ [45, 68], and the dimensionless electronic spine density $\overline{n} = \lambda^2 \overline{N}$, Eq. (2.3) can be rewritten as

$$\tau_m \partial_t V_H = \lambda^2 \nabla^2 V_H + \overline{n} R_s I_{ss} - I_{ion} R_m. \tag{2.3}$$

A horizontal cell spine head around point (x, y) is modeled as an isopotential compartment with surface area A_{sh} $(\mu\mathrm{m}^2)$ and specific membrane capacitance C_m, and its membrane potential U_H (mV) satisfies the following current balance equation

$$C_{sh}\,\partial_t U_H = -I_{ss} - I_{syn} - A_{sh} I_{ion} \tag{2.4}$$

where $C_{sh} = A_{sh} C_m$ $(\mu\mathrm{F})$ is the capacitance of an individual spine head, I_{ss} is the same as given in Eq. (2.2), the ionic current density I_{ion} will be given later in Eqs. (2.7) $\sim$(2.10), and the synaptic current I_{syn} , activated by transmitter glutamate released from the cone, is defined as

$$I_{syn} = g_{syn}(U_H - E_{syn}) \tag{2.5}$$

where the synaptic conductance g_{syn} (pS) is set to be proportional to the value of $[GL]$ $(\mu\mathrm{M})$, the extracellular concentration of glutamate, and the synaptic reversal potential E_{syn} is around zero for glutamate synapse [56]. Hence, the synaptic current can be rewritten as

$$I_{syn} = (k_{syn}[GL])U_H \tag{2.6}$$

where k_{syn} is a scaling factor $(\mathrm{pS}/\mu\mathrm{M})$.

An evident feature of this continuum formulation of horizontal cells which can be seen in Eqs. (2.3)$\sim$(2.4) is that there is no direct electrical communication between neighboring spines and hence the voltage spread along the horizontal cell slab is the only way through which the spines can interact with each other [5].

The ionic current density I_{ion} in Eq. (2.3) and (2.4) consists of a linear leakage current I^H_{leak} and a nonlinear inward "sag" current I_{sag}. I_{sag} is included in the model in order to account for the transient "sag" and PIR observed in the voltage recordings of horizontal cells introduced in the previous chapter, and its ex-

pression evolves from a model of the T-type calcium current in thalamic neurons [141, 140]. In fish and mammalian retinal horizontal cells, T-type or T-type-like calcium currents were reported [74, 97, 108, 123] together with N-type, L-type and other types of calcium currents, sodium current, and various types of potassium currents [74, 108, 130]. Specifically, I_{ion} takes the following form

$$I_{ion}(V,h) = I^H_{leak} + I_{sag} \tag{2.7}$$

where

$$I^H_{leak} = (V - E_{LH})g_{LH}, \qquad I_{sag} = (V - E_{sag})g_{sag}h \tag{2.8}$$

In Eq. (2.8), E_{LH} (mV) and E_{sag} (mV) are the reversal potentials for I^H_{leak} and I_{sag}, respectively; and g_{LH} (nS/cm^2) and g_{sag} (nS/cm^2) are the corresponding conductances for I^H_{leak} and I_{sag}. The inactivation gating variable h in I_{sag} is governed by

$$\tau_h \, \partial_t h = h_\infty(V) - h \tag{2.9}$$

$$h_\infty(V) = [1 + e^{-(V-\theta_h)/\sigma_h}]^{-1} \tag{2.10}$$

with τ_h being a constant. The symbols V and h in the above equations stand for the actual state variables V_H and h_V in I_{ion} of Eq. (2.3) and the actual state variables U_H and h_U in I_{ion} of Eq. (2.4). We noticed that, although some studies use the 'sag' or 'rollback' response of horizontal cells as an index of feedback [51, 138, 31], it was also suggested that the 'sag' response is not a sensitive measure of feedback [44]. In the present model, 'sag' is not taken as a feedback index.

The concentration of the calcium-blocking agent GABA released by horizontal cells into the intersynaptic cleft, is denoted by [G] (μM), and is modeled as

$$\tau_G \, \partial_t [G] = k_G(U_H - E_G) \tag{2.11}$$

where

$$E_G = \left(\frac{RT}{F}\right)\frac{\ln\left([G]/[G_i]\right)}{n_i} = \left(\frac{RT}{F}\ln(10)\right)\frac{\log_{10}\left([G]/[G_i]\right)}{n_i}. \tag{2.12}$$

τ_G and k_G in Eq. (2.11) are the time constant and scaling factor for GABA kinetics, respectively. Based on the fact that the release of GABA is voltage-dependent [110, 111], GABA is treated as a n_i-charged particle whose balance between its extracellular concentration $[G]$ and intracellular concentration $[G_i]$ is controlled by the difference between U_H, the membrane potential of horizontal cell spine head, and E_G, the Nernst-type "reversal potential" of GABA. Eqs. (2.11)$\sim$(2.12) are for reverse transport of GABA (i.e., non-vesicular GABA release) since they model both the GABA release from and reuptake into horizontal cells as membrane transport processes [112]. In Eq. (2.12), R is the gas constant (8.314 $\mathrm{J}\cdot\mathrm{mol}^{-1}\cdot\mathrm{K}^{-1}$), T is the temperature (in K), and F is Faraday constant (96485 $\mathrm{C}\cdot\mathrm{mol}^{-1}$). At a temperature of 19 °C , $\frac{RT}{F}\ln(10) = 58$ mV.

2.2 The cones

The cone membrane potential V_C (mV) satisfies the following current balance equation

$$C_m\,\partial_t V_C = -I^C_{leak} + I_{dark} + I_{flick} + I_{bkgd} \tag{2.13}$$

where

$$I^C_{leak} = (V_C - E_{LC})g_{LC} \tag{2.14}$$

is the density of a leakage current ($\mu\mathrm{A}/\mathrm{cm}^2$) with reversal potential E_{LC} (mV) and conductance g_{LC} (nS/cm^2). I_{dark} ($\mu\mathrm{A}/\mathrm{cm}^2$) is the density of a constant "dark" current representing a steady inward cation current mainly contributed by sodium ions that depolarizes photoreceptor membrane potential in darkness [10, 35, 39, 149]. I_{flick} ($\mu\mathrm{A}/\mathrm{cm}^2$) is the current density transduced by a cone-selective flicker

stimulus applied to a region S around the center of a patch of isolated retina tissue on the xy-plane and has the form of a periodic "square" wave shown in Fig. 2 (b). I_{bkgd} (μA/cm^2) is the density of the current generated by a rod-selective diffusive background illumination, which enters the cone through rod-cone gap junctions [86]. The value of I_{dark} is given in Table 3 and the expressions for I_{flick} and I_{bkgd} are given in Section 2.3.

The cone calcium current I_{Ca} (pA) is governed by

$$\tau_{Ca}\,\partial_t I_{Ca} = \frac{(V_C - \alpha U_H - E_{Ca})g_{Ca}}{(1+e^{-(V_C-\alpha U_H-A)/B})(1+k_{OCa}[G])} - I_{Ca} \tag{2.15}$$

where $I_{Ca} < 0$ since the current is inward, τ_{Ca} (ms) is the time constant, E_{Ca} (mV) is the reversal potential, and g_{Ca} (nS) is the maximum conductance . Here I_{Ca} should be considered as a point current at (x,y) activated by a single cone-horizontal cell synaptic contact around that point. The first term on the right-hand-side of Eq. 2.15 contains a linear current factor $(V_C - \alpha U_H - E_{Ca})g_{Ca}$ multiplied by a sigmoidal activation function $1/(1+e^{-(V_C-\alpha U_H-A)/B})$ where A (mV) is the half saturation voltage and B (mV) is a slope factor. The expression of such a product is modified from published models on photoreceptor I_{Ca} [8, 135, 44]. The linear term $-\alpha U_H$ with α being a scaling parameter shifts the cone Ca^{2+} current-voltage relationship to more negative values of V_C when the horizontal cell is hyperpolarized (i.e., when U_H becomes more negative), which is consistent with the ephaptic hypothesis [135, 48, 44] and with the reported nearly linear shift of cone calcium current activation potential induced by horizontal cell hyperpolarization [31, 63]. The expression $1/(1+k_{OCa}[G])$ is derived from a Hill function on the binding kinetics of GABA to open calcium channels, and represents the fraction of open calcium channels as a function of extracellular GABA concentration $[G]$ with k_{OCa} ($1/\mu$M) being the binding constant [152]. Thus, the product of the maximum conductance g_{ca}

and the fraction $1/(1+k_{OCa}[G])$ reflects the GABA-mediated modulation of cone calcium conductance. The last term stands for the removal of calcium from the cone by either extrusion to extracellular space or binding to intracellular stores. A novel feature of the model is that Eq. (2.15) contains both GABAergic and non-GABAergic mechanisms, which enables us to investigate these two feedback effects separately as well as jointly.

Although the calcium current I_{Ca} modeled in Eq. (2.15) flows into the cone and it is mentioned in the previous chapter that cone has calcium-activated chloride current $I_{Cl(Ca)}$, these two currents are not included in Eq. (2.13) of cone membrane potential for the following reasons. First, the effect of I_{Ca} on cone membrane potential is assumed to be small since the calcium conductance is small relative to the total membrane conductance of the cone [62, 135]. Second, it was suggested that, under physiological conditions, the depolarizing effect of I_{Ca} on cone membrane potential could be counteracted by the hyperpolarizing effect of $I_{Cl(Ca)}$ [52, 62, 135]. Third, experiments indicate that feedback induced polarization of cone membrane potential, if there is any, is not essential for the transmission of the feedback signal to second-order neurons; rather, it is the direct modulation of cone's I_{Ca} (hence intracellular calcium concentration) and the subsequent glutamate release that affects the responses of second-order neurons [15, 52, 62].

The rate of release of glutamate from the cone pedicle into the intersynaptic cleft depends linearly on I_{Ca} [106, 128, 144] and is described by

$$\tau_{GL}\,\partial_t[GL] = -k_{Ca}I_{Ca} - [GL] \tag{2.16}$$

where $[GL]$ (μM) is the concentration of glutamate in the cleft. In this equation, the time rate of change of glutamate is balanced by its release triggered by the inward cone calcium current ($I_{Ca} < 0$) and its uptake by transporters.

2.3 The overall model

In summary, the continuum two-dimensional model for the cone-horizontal cell interaction takes the following form

$$\begin{aligned}
\tau_m \partial_t V_H &= \lambda^2 \nabla^2 V_H + \frac{\overline{n} R_s}{R_{ss}}(U_H - V_H) \\
&\quad -[(V_H - E_{LH}) g_{LH} + (V_H - E_{sag}) g_{sag} h_V] R_m \qquad (2.17) \\
C_{sh} \partial_t U_H &= -\frac{(U_H - V_H)}{R_{ss}} - k_{syn}[GL] U_H \\
&\quad -A_{sh}[(U_H - E_{LH}) g_{LH} + (U_H - E_{sag}) g_{sag} h_U] \qquad (2.18) \\
C_m \partial_t V_C &= -(V_C - E_{LC}) g_{LC} + I_{dark} + I_{flick} + I_{bkgd} \qquad (2.19) \\
\tau_G \partial_t [G] &= k_G \Big(U_H - (RT/F) \frac{\ln([G]/[G_i])}{n_i} \Big) \qquad (2.20) \\
\tau_{Ca} \partial_t I_{Ca} &= \frac{(V_C - \alpha U_H - E_{Ca}) g_{Ca}}{(1 + e^{-(V_C - \alpha U_H - A)/B})(1 + k_{OCa}[G])} - I_{Ca} \qquad (2.21) \\
\tau_{GL} \partial_t [GL] &= -k_{Ca} I_{Ca} - [GL] \qquad (2.22) \\
\tau_h \partial_t h_V &= \frac{1}{1 + e^{-(V_H - \theta_h)/\sigma_h}} - h_V \qquad (2.23) \\
\tau_h \partial_t h_U &= \frac{1}{1 + e^{-(U_H - \theta_h)/\sigma_h}} - h_U \qquad (2.24)
\end{aligned}$$

where each state variable depends on x, y and t. The applied currents I_{flick} and I_{bkgk} in Eq. (2.19) for V_C are defined with respect to a general two-dimensional flicker stimulus region S as

$$I_{flick}(x,y,t) = \begin{cases} A_{flick} H\big(z(t), \beta_1\big) & \text{if } (x,y) \in S \;\&\; t \in [t_{beg}^{flick},\, t_{end}^{flick}] \\ 0 & \text{elsewhere} \end{cases} \qquad (2.25)$$

and

$$I_{bkgd}(x,y,t) = \begin{cases} \gamma A_{bkgd} H(t - t_{beg}^{bkgd}, \beta_2) H(t_{end}^{bkgd} - t, \beta_3) & \text{if } (x,y) \in S \\ A_{bkgd} H(t - t_{beg}^{bkgd}, \beta_2) H(t_{end}^{bkgd} - t, \beta_3) & \text{if } (x,y) \in S^c \end{cases} \qquad (2.26)$$

where S is typically a connected region on the plane and can be defined in polar coordinates as

$$S = \{(r,\theta) : b(\theta) \le r \le a(\theta), \theta \in [0, 2\pi]\}$$

for some general functions $a(\theta)$ and $b(\theta)$. The various shapes of S studied in this project are shown in Fig. 2. The functions H and z in Eqs. (2.25) and (2.26) are defined as

$$H(w,\beta) = \frac{1+\tanh(\beta w)}{2} \tag{2.27}$$

and

$$z(t) = \sin\left(\frac{2\pi}{P}(t - t_{beg}^{flick})\right) \tag{2.28}$$

where β is the slope factor and P is the period of the "square" wave flicker stimulus. The composition of H and z in the expression of I_{flick} in Eq. (2.25) generates the smooth periodic "square" wave shown in Fig. 2 (b).

To account for the saturation desensitization of rods at their exposure to the bright flicker [96] to some extent, in Eq. (2.26), the magnitude of the background-induced rod-mediated current density I_{bkgd} inside the flicker stimulus region S is reduced to a fraction γ of the magnitude of I_{bkgd} outside S (see also Fig. 2 (d)). The expression of γ is given by

$$\gamma = \frac{b_\gamma}{1+\exp\left((a-\theta_{tst})/\sigma_{tst}\right)} \tag{2.29}$$

where a is the half width of a slit or square stimulus region, or the radius of a disk stimulus region. The values of the kinetic parameters b_γ, θ_{tst} and σ_{tst} are determined by fitting the model to experimental data, and are summarized in Table 1. Plots of γ for different stimulus regions are displayed in Fig. 1. Here γ is formulated as a monotonically decreasing function of the size of S (in terms of a) by the assumption that the smaller S is, the easier it is for the background-induced current outside but in the immediate neighborhood of S to flow into S (through gap-junctions between photoreceptors) to compensate for the reduction of I_{bkgd} due to rod desensitization in this region. It will be shown in Fig. 13 of Chapter 4 that the expression for γ as a function of a in Eq. (2.29) is necessary for the computational

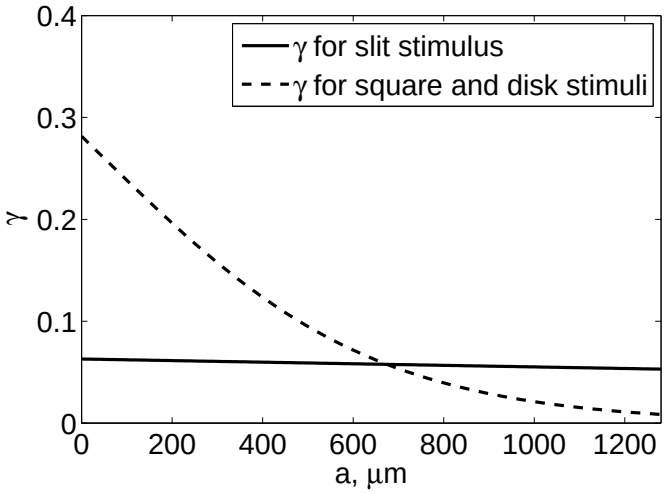

Figure 1: γ as a function of a for different stimulus regions.

results of the model with square stimulus (and disk stimulus) to get good fits with the corresponding experimental data, while a constant value of γ (e.g., 0.05$\sim$0.1) can work well for slit stimulus. Introducing the function γ also into the model with a slit stimulus provides a possible unified framework for the model with different stimulus regions.

As shown in Fig. 2 (d), the offset speed of I_{bkgd} is set to be evidently slower than its onset speed to account for the rod after-effect, namely, the slow return of the rod-induced hyperpolarization towards its baseline after the background is turned off [119, 118, 98]. The spatial transitions of the currents I_{flick} and I_{bkgd} across the stimulus region S studied in this project are also modeled as smooth curves as shown in Fig. 2 (f), and expressions of these two currents defined for specific S are given in Chapter 3. Steady-state values of the state variables in the absence of I_{flick} and I_{bkgd}, which are taken as the initial conditions, are listed in Table 2. Reference parameter values for Eqs. (2.17)$\sim$(2.28) are listed in Table 3$\sim$5.

Table 1: Parameter values in the expression of γ for different stimuli.

Symbol	slit	square	disk
b_γ	0.125	0.52	0.52
θ_{tst}	50 μm	50 μm	50 μm
σ_{tst}	4000 μm	300 μm	300 μm

Table 2: Initial values of state variables.

Variable	Initial value	Unit	Description
V_H	-28.32	mV	membrane potential of HC slab
U_H	-28.24	mV	membrane potential of HC spine head
V_C	-25.33	mV	membrane potential of cone
$[G]$	1.629	μM	extracellular concentration of GABA
I_{Ca}	-1.375	pA	cone calcium current
$[GL]$	20.62	μM	extracellular concentration of glutamate
h_V	0.3321	–	gating variable of I_{sag} in HC slab
h_U	0.3250	–	gating variable of I_{sag} in HC spine head

Table 3: Supplied reference parameter values for the model.

Symbol	Value	Unit	Description
α	0.88	–	ephaptic coefficient
θ_h	-30	mV	threshold of h_∞ for gating variable h
σ_h	-2.4	mV	slope factor of h_∞ for gating variable h
τ_{Ca}	5	ms	time constant for I_{Ca}
τ_G	15	ms	time constant for GABA release
τ_{GL}	18.18	ms	time constant for glutamate release
τ_h	800	ms	time constant for gating variable h
A	-40.8	mV	half saturation voltage of I_{Ca}
A_{sh}	1.31	μm^2	average surface area of a spine head
B	3	mV	activation slope of I_{Ca}
C_m	1	μF/cm^2	specific membrane capacitance
D_{ss}	0.1	μm	HC spine stem diameter
E_{Ca}	120	mV	reversal potential for I_{Ca}
E_{LC}	-68	mV	cone leak potential
E_{LH}	-60	mV	HC leak potential
E_{sag}	120	mV	reversal potential for I_{sag}
F	96485	C $\cdot$ mol^{-1}	Faraday constant
g_{Ca}	0.03	nS	peak conductance of I_{Ca}
g_{LC}	1.5×10^5	nS/cm^2	cone leak conductance
g_{LH}	1×10^5	nS/cm^2	HC leak conductance
g_{sag}	1.7×10^4	nS/cm^2	conductance for I_{sag}
$[G_i]$	5	μM	intracellular concentration of GABA
I_{dark}	6.4	μA/cm^2	cone dark current
k_{Ca}	15	μM/pA	scale factor for glutamate release
k_G	1	μM/mV	scale factor for GABA release
k_{OCa}	1	1/μM	binding equilibrium constant for GABA
k_{syn}	0.1572	pS/μM	scale factor for I_{syn}
L	1280	μm	half side-length of HC slab
L_{ss}	5	μm	HC spine stem length
n_i	1	–	number of charges per GABA molecule
$\overline{N}$	3.84×10^7	1/cm^2	physical spine density
R	8.314	J $\cdot$ mol^{-1} $\cdot$ K^{-1}	gas constant
R_i	200	$\Omega\cdot$cm	intracellular resistivity of a spine stem
R_s	12	MΩ	sheet resistance of HC slab
T	292.15	K	temperature

Table 4: Computed reference parameter values for the model.

Symbol	Formula	Value	Unit	Description
C_{sh}	$C_m A_{sh}$	0.0131	pF	spine head capacitance
R_m	$1/g_{LH}$	10^4	$\Omega \cdot \mathrm{cm}^2$	passive membrane resistivity
R_{ss}	$(4L_{ss}R_i)/(\pi D_{ss}^2)$	1273.24	MΩ	spine stem resistance
λ	$\sqrt{R_m/R_s}$	288.675	μm	HC slab length constant
τ_m	$R_m C_m$	10	ms	membrane time constant
$\overline{n}$	$\lambda^2 \overline{N}$	3.2×10^4	–	electronic spine density

Table 5: Reference parameter values for I_{flick} and I_{bkgd}.

Symbol	Value	Unit	Description
β_1	50	–	onset-/offset- speed in each flicker cycle of I_{flick}
β_2	0.15	ms^{-1}	onset speed of I_{bkgd}
β_3	0.01	ms^{-1}	offset speed of I_{bkgd}
β_4	0.28	$\mu\mathrm{m}^{-1}$	spatial transition slope of I_{flick} and I_{bkgd} across S
A_{flick}	-7.15	$\mu\mathrm{A/cm}^2$	hyperpolarizing amplitude of I_{flick}
A_{bkgd}	-7	$\mu\mathrm{A/cm}^2$	hyperpolarizing amplitude of I_{bkgd} exterior to S
P	62.5	ms	period of the "square" wave flicker stimulus
t_{beg}^{flick}	900	ms	time to turn on flicker stimulus
t_{end}^{flick}	4564.29	ms	time to turn off flicker stimulus
t_{beg}^{bkgd}	2121.43	ms	time to turn on background illumination
t_{end}^{bkgd}	3342.86	ms	time to turn off background illumination

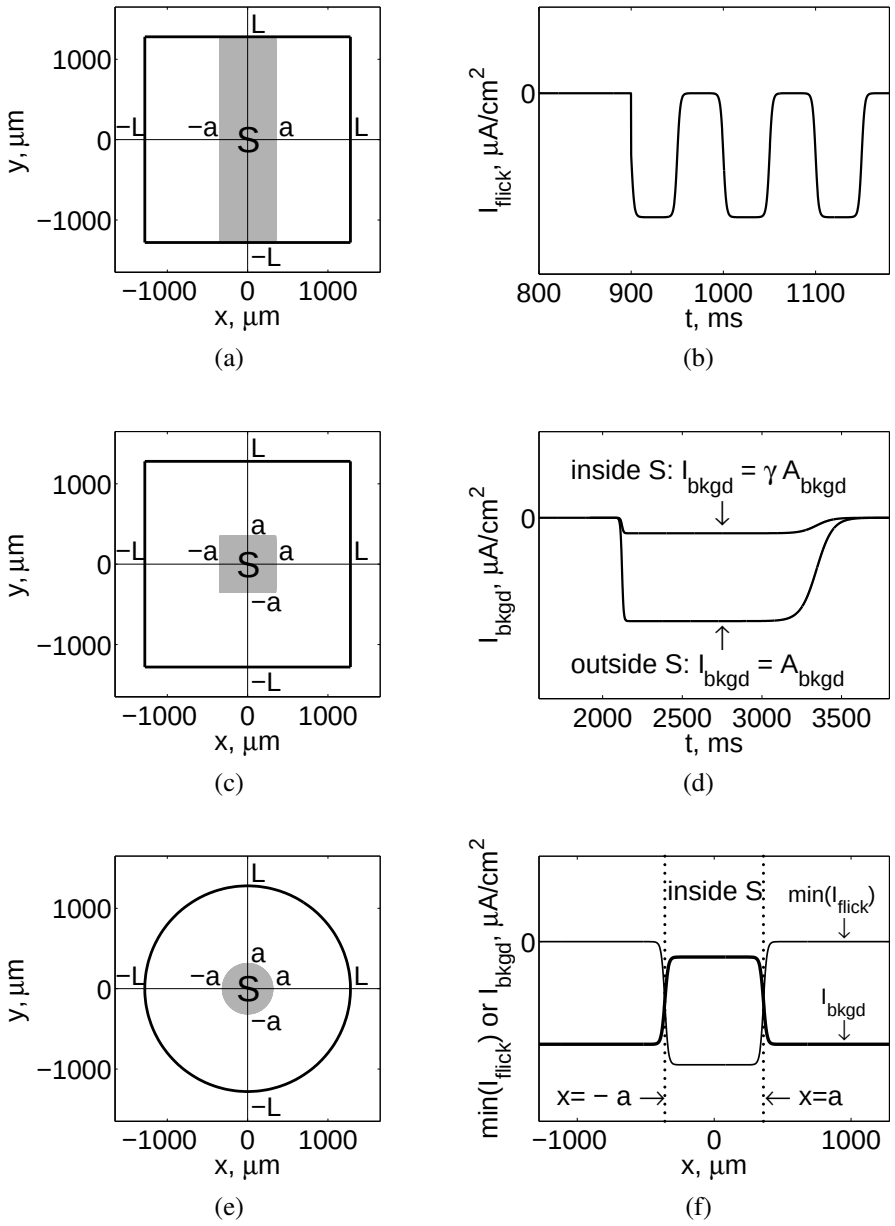

Figure 2: Spatial geometries of the modeled retina patches and the temporal and spatial characteristics of I_{flick} and I_{bkgd}. (a), (c) and (e): modeled retina patches occupy the regions inside the thick solid boundaries with the gray areas at the center representing the slit, square and disk flicker stimulus region S, respectively. (b): a few cycles of the "square" wave flicker stimulus I_{flick} inside region S. The parameter β_1 is reduced to 1/10 of its actual value to magnify the smooth shape of the wave form. (d): the background-induced current I_{bkgd} inside and outside region S as a function of time. (f): $\min(I_{flick})$ and I_{bkgd} as a function of x for $y = 0$. The parameter β_4 is reduced to 1/7 of its actual value to magnify the smooth transition of the two currents across the boundaries of region S.

CHAPTER 3

NUMERICAL METHOD

The model is solved by method of lines. Specifically, the PDE model is first discretized in space using central differences for the spatial derivatives. This generates a system of ordinary differential equations (ODEs) at each grid point, which is then solved using MATLAB's built-in stiff ODE solver ode23tb, an L-stable implicit Runge-Kutta method implementing the TR-BDF2 algorithm [81]. The method is second order accurate in both space and time [72]. This chapter focuses on the spatial discretization of the PDE model using finite difference methods since the solution of the resulting ODE system by MATLAB's built-in ODE solver is fairly routine.

3.1 Numerical method for the model with a slit stimulus

The model to be solved is defined generally over a rectangular region

$$\Omega = \{(x,y) : x \in [-L_x,\, L_x],\; y \in [-L_y,\, L_y]\} \tag{3.1}$$

with homogeneous Neumann boundary conditions and has a flickering stimulus region along a vertical slit

$$S = \{(x,y) : x \in [-a,\, a],\; y \in [-L_y,\, L_y],\; a < L_x, L_y\}. \tag{3.2}$$

Fig. 2 (a) gives a schematic illustration of the spatial geometry of the modeled region with the simplified setting $L_x = L_y = L$. If the slit is long enough (i.e., if L_y is sufficiently large), then, as recognized by Nelson [86], the solution of the model above can be approximated quite well by that with a flickering slit of infinite length given by

$$S = \{(x,y) : x \in [-a,\, a], y \in (-\infty,\, \infty),\; a < L_x\}. \tag{3.3}$$

Assuming that I_{flick}, I_{bkgd} and all parameters are constant in the y-direction, the first derivative with respect to y of each state variable in the model with S defined in Eq. (3.3) vanishes. This reduces the model to one spatial dimension along the x-axis. In particular, the Laplacian in Eq. (2.17) is replaced by

$$\nabla^2 V_H = \frac{\partial^2 V_H}{\partial x^2} \tag{3.4}$$

since $\partial^2 V_H / \partial y^2 = 0$, and the model equations, (2.17)$\sim$(2.24), remain the same except that the state variables do not depend on y any more. This one-dimensional reduction saves computational time considerably compared to solving the model over a two-dimensional region. The computational work is further reduced by taking advantage of the model's symmetry about the y-axis and considering its solution only for

$$x \in \Omega = [0,\ L_x] := [0,\ L] \quad \text{and} \quad S = [0,\ a] \text{ where } a < L. \tag{3.5}$$

Homogeneous Neumann boundary condition remains unchanged at $x = L$ and is imposed at the origin to preserve the symmetry; hence,

$$\left.\frac{\partial V_H}{\partial x}\right|_{x=0} = 0 \quad \text{and} \quad \left.\frac{\partial V_H}{\partial x}\right|_{x=L} = 0. \tag{3.6}$$

The input currents I_{flick} and I_{bkgd} are now defined for $x \in [0,\ L]$ as

$$I_{flick}(x,t) = \begin{cases} A_{flick} H\big(z(t), \beta_1\big) H\big(a-x, \beta_4\big) & \text{for } t \in [t_{beg}^{flick},\ t_{end}^{flick}] \\ 0 & \text{for } t \text{ elsewhere} \end{cases} \tag{3.7}$$

and

$$I_{bkgd}(x,t) = A_{bkgd} H(t - t_{beg}^{bkgd}, \beta_2) H(t_{end}^{bkgd} - t, \beta_3) \Big(\gamma + (1-\gamma) H(x-a, \beta_4)\Big). \tag{3.8}$$

Note that the transitions of I_{flick} and I_{bkgd} across the stimulus region S are endowed by the smooth function H defined previously in Eq. (2.27).

With the computational domain Ω given in Eq. (3.5), the model is solved over $N+1$ equispaced points at

$$x_i = (i-1)h \quad \text{for} \quad i = 1:N+1 \tag{3.9}$$

where

$$h = L/N \tag{3.10}$$

is the mesh width, the distance between grid points. To take care of the boundary conditions, introduce fictitious points x_i for $i = 0$ and $i = N+2$ in Eq. (3.9). Letting $V_H(i)$ denote the numerical value of V_H computed at x_i and approximating the first and second spatial derivatives by centered differences, we have

$$\frac{\partial V_H(i)}{\partial x} \approx \frac{V_H(i+1) - V_H(i-1)}{2h} \quad \text{for} \quad i = 1:N+1 \tag{3.11}$$

and

$$\frac{\partial^2 V_H(i)}{\partial x^2} \approx \frac{V_H(i-1) - 2V_H(i) + V_H(i+1)}{h^2} \quad \text{for} \quad i = 1:N+1. \tag{3.12}$$

Eq. (3.11) and the boundary conditions in Eq. (3.6) imply that

$$V_H(i=0) = V_H(i=2) \quad \text{and} \quad V_H(i=N+2) = V_H(i=N). \tag{3.13}$$

Combining the results in Eqs. (3.12) and (3.13), the second differential operator in Eq. (3.4) with homogeneous Neumann boundary conditions is then given, in the discretized form, by the following $(N+1)\times(N+1)$ differentiation matrix

$$\frac{\partial^2}{\partial x^2} \approx D_x^2 = \frac{1}{h^2}\begin{bmatrix} -2 & 2 & & & \\ 1 & -2 & 1 & & \\ & \ddots & \ddots & \ddots & \\ & & 1 & -2 & 1 \\ & & & 2 & -2 \end{bmatrix}. \tag{3.14}$$

3.2 Numerical method for the model with a square stimulus

The model is defined generally over a rectangular region Ω given in Eq. (3.1) with homogeneous Neumann boundary conditions and has a square flickering stimulus region S given by

$$S = \{(x,y) : x \in [-a,\ a],\ y \in [-a,\ a],\ a < L_x, L_y\}. \tag{3.15}$$

For simplicity, we set $L_x = L_y = L$ in Eq. (3.1) and (3.15), and illustrate the regions Ω and S in Fig. 2 (c). By symmetry of the model about the x- and y- axes, it's sufficient to solve it over the following computational domain

$$\Omega = \{(x,y) : x \in [0,\ L],\ y \in [0,\ L]\} \tag{3.16}$$

with flickering stimulus over the region

$$S = \{(x,y) : x \in [0,\ a],\ y \in [0,\ a],\ a < L\}. \tag{3.17}$$

Homogeneous Neumann boundary conditions remain unchanged at $x = L$ or $y = L$ and are imposed at $x = 0$ or $y = 0$ to preserve the symmetry. Thus we have

$$\left.\frac{\partial V_H}{\partial x}\right|_{x=0} = \left.\frac{\partial V_H}{\partial x}\right|_{x=L} = \left.\frac{\partial V_H}{\partial y}\right|_{y=0} = \left.\frac{\partial V_H}{\partial y}\right|_{y=L} = 0. \tag{3.18}$$

Letting $T_{flick} = [t_{beg}^{flick},\ t_{end}^{flick}]$, the input currents I_{flick} and I_{bkgd} are now defined for $(x,y) \in [0,\ L] \times [0,\ L]$ as

$$I_{flick}(x,y,t) = \begin{cases} A_{flick} H\big(z(t), \beta_1\big) H\big(a-x, \beta_4\big) H\big(a-y, \beta_4\big) & \text{for } t \in T_{flick} \\ 0 & \text{for } t \text{ elsewhere} \end{cases}$$

and

$$\begin{aligned} I_{bkgd}(x,y,t) = {} & A_{bkgd} H(t - t_{beg}^{bkgd}, \beta_2) H(t_{end}^{bkgd} - t, beta_3) \\ & \times \Big(\gamma + (1-\gamma) F_2\Big(H(x-a,\beta_4), H(y-a,\beta_4)\Big)\Big) \end{aligned}$$

where the function F_2 is defined as

$$F_2(p,q) = \frac{|p+q| + |p-q|}{2}. \tag{3.19}$$

Note that if $p, q \in \{0,1\}$, then the function F_2 defined in Eq. (3.19) is equivalent to the logic OR operation given by

$$(p \,|\, q) \tag{3.20}$$

or by

$$(p > 0.5 \,|\, q > 0.5). \tag{3.21}$$

But if we set

$$p = H(x-a, \beta_4) \quad \text{and} \quad q = H(y-a, \beta_4), \tag{3.22}$$

then neither of two operations given in Eqs. (3.20)$\sim$(3.21) will be a smooth function of x and y and the operation given in Eq. (3.20) even fails to define accurately S^c, the region outside of the stimulus region. In contrast, the composition of the functions in Eq. (3.19) and (3.22) given by

$$F_2\Big(H(x-a, \beta_4), H(y-a, \beta_4)\Big) \tag{3.23}$$

has the computationally desirable feature of being a smooth function of x and y and defines the region S^c quite well. In other words, the composite function defined in Eq. (3.23) is essentially a smooth version of a two-dimensional heaviside function (see Fig. 3).

The model is solved over $(N+1) \times (N+1)$ equispaced grid points $(x_i,\ y_j)$ given by

$$x_i = (i-1)h,\ \ y_j = (j-1)h \quad \text{for} \quad i, j = 1 : N+1 \tag{3.24}$$

where the one-dimensional mesh width h is the same as given in Eq. (3.10). To take care of the boundary conditions, introduce fictitious points (x_i, y_j) whose coordi-

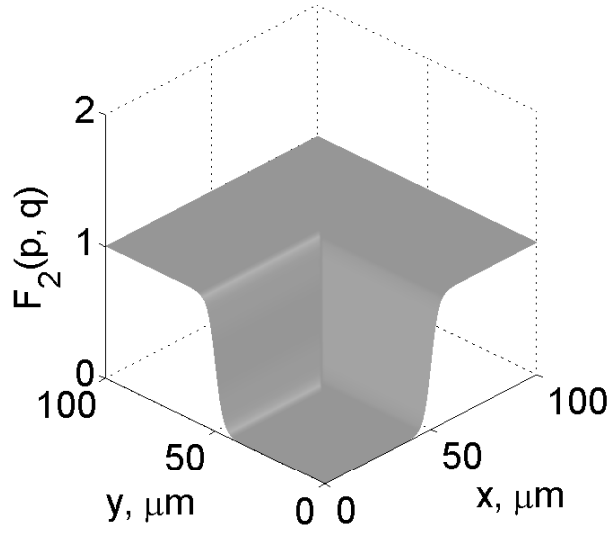

Figure 3: The smooth two-dimensional heaviside function defined in Eq. (3.23). In the plot, $F_2(p,\ q)$ is a smooth function of x and y where $p = H(x-a,\ \beta_4)$ and $q = H(y-a,\ \beta_4)$ with $a = 50\ \mu$m, $\beta_4 = 0.28\ \mu\text{m}^{-1}$. The flicker stimulus region S is defined in Eq. (3.15). The majority of points in the region S have function values very close to zero while the majority of points in the region S^c have function values very close to 1.

nates are defined in Eq. (3.24) and whose indices are given as follows

$$(i=0,\ j) \ \text{ and } \ (i=N+2,\ j) \quad \text{for} \quad j=1:N+1$$

$$(i,\ j=0) \ \text{ and } \ (i,\ j=N+2) \quad \text{for} \quad i=1:N+1.$$

Letting $V_H(i,j)$ denote the numerical value of V_H computed at the grid point (x_i, y_j) and approximating the first spatial derivatives by centered difference similar to the one given in Eq. (3.11), we derive from the boundary conditions given in Eq. (3.18)

that

$$V_H(i=0,\ j) = V_H(i=2,\ j) \quad \text{for} \quad j = 1:N+1 \tag{3.25}$$

$$V_H(i=N+2,\ j) = V_H(i=N,\ j) \quad \text{for} \quad j = 1:N+1 \tag{3.26}$$

$$V_H(i,\ j=0) = V_H(i,\ j=2) \quad \text{for} \quad i = 1:N+1 \tag{3.27}$$

$$V_H(i,\ j=N+2) = V_H(i,\ j=N) \quad \text{for} \quad i = 1:N+1. \tag{3.28}$$

With the second spatial derivatives computed by centered difference similar to the one given in Eq. (3.12), the Laplacian in Eq. (2.17) on the discrete grid is approximated, for $i, j = 1:N+1$, by the following expression

$$\begin{aligned} & \nabla^2 V_H(i,j) \\ &= \left(\frac{\partial^2}{\partial x^2} + \frac{\partial^2}{\partial y^2}\right) V_H(i,j) \\ &\approx (D_x^2 + D_y^2) V_H(i,j) \\ &= \frac{1}{h^2}\Big(V_H(i-1,j) + V_H(i+1,j) + V_H(i,j-1) + V_H(i,j+1) - 4V_H(i,j)\Big) \end{aligned} \tag{3.29}$$

where the values of V_H at fictitious points, whenever they appear, are replaced by their equivalent values at true grid points as listed in Eqs. (3.25)$\sim$(3.28).

Putting the values $V_H(i,j)$ for $i, j = 1:N+1$ into a column vector of length $(N+1)^2$ by redefining

$$V_H\big(i + (j-1)(N+1)\big) := V_H(i,j), \tag{3.30}$$

the discrete two-dimensional Laplacian operator in Eq. (3.29) with homogeneous Neumann boundary conditions can be written as a $(N+1)^2 \times (N+1)^2$ matrix. For example, when $N = 2$, the discrete operator with homogeneous Neumann boundary

conditions is a 9×9 matrix given by

$$\frac{\partial^2}{\partial x^2}+\frac{\partial^2}{\partial y^2} \approx D_x^2+D_y^2 = \frac{1}{h^2}\begin{bmatrix} -4 & 2 & & 2 & & & & & \\ 1 & -4 & 1 & & 2 & & & & \\ & 2 & -4 & 0 & & 2 & & & \\ 1 & & 0 & -4 & 2 & & 1 & & \\ & 1 & & 1 & -4 & 1 & & 1 & \\ & & 1 & & 2 & -4 & 0 & & 1 \\ & & & 2 & & 0 & -4 & 2 & \\ & & & & 2 & & 1 & -4 & 1 \\ & & & & & 2 & & 2 & -4 \end{bmatrix}$$

where all the entries not shown are zeros.

3.3 Numerical method for the model with a disk stimulus

For convenience, use polar coordinates and define the model over a circular region (Fig. 2 (e))

$$\Omega = \{(r,\theta) : r \in [0,\ L],\ \theta \in [0,\ 2\pi]\} \tag{3.31}$$

with flickering stimulus applied on a disk

$$S = \{(r,\theta) : r \in [0,\ a],\ \theta \in [0,\ 2\pi],\ a < L\} \tag{3.32}$$

and the boundary condition

$$\left.\frac{\partial V_H}{\partial r}\right|_{r=L} = 0. \tag{3.33}$$

By symmetry, the model can be reduced to one spatial dimension for any fixed θ. Setting $\theta = 0$ and replacing r by x in Eqs. (3.31)$\sim$(3.33), the computational domain Ω, the stimulus region S, the input currents I_{flick} and I_{bkgd} now all have exactly the same forms as given in Eq. (3.5), (3.7) and (3.8), respectively; the boundary conditions are also identical with those expressed in Eq. (3.6) where the symmetry at the

origin is preserved for this disk stimulus model; and the Laplacian in Eq. (2.17) is replaced by

$$\nabla^2 V_H = \frac{\partial^2 V_H}{\partial x^2} + \frac{1}{x}\frac{\partial V_H}{\partial x}. \tag{3.34}$$

The model system is still the same as given in Eqs. (2.17)$\sim$(2.24) except that all state variables here are functions of x and t only.

The model is solved numerically over N staggered grid points

$$x_i = \frac{h}{2} + (i-1)h \quad \text{for} \quad i = 1:N \tag{3.35}$$

where the mesh width h is the same as defined in Eq. (3.10). To take care of the boundary conditions, introduce fictitious points x_i for $i = 0$ and $i = N+1$ in Eq. (3.35). The boundary conditions given in Eq. (3.6) can now be approximated respectively by

$$0 = \left.\frac{\partial V_H}{\partial x}\right|_{x=0} \approx \frac{V_H(i=1) - V_H(i=0)}{h} \tag{3.36}$$

and

$$0 = \left.\frac{\partial V_H}{\partial x}\right|_{x=L} \approx \frac{V_H(i=N+1) - V_H(i=N)}{h} \tag{3.37}$$

which imply that[1]

$$V_H(i=0) = V_H(i=1) \quad \text{and} \quad V_H(i=N+1) = V_H(i=N). \tag{3.38}$$

The first and second derivatives at true grid points are still approximated by the centered difference formulae given in Eqs. (3.11) and (3.12), except that the index i now goes from 1 to N. Combining the results in Eq. (3.38) and in Eqs. (3.11)$\sim$(3.12) for $i = 1:N$, the first and second differential operators in Eq. (3.34) with homogeneous Neumann boundary conditions are then given, in the discretized form, by the

[1]The relation $V_H(i=0) = V_H(i=1)$ can also be obtained directly by symmetry about the origin.

following $N \times N$ differentiation matrices, respectively

$$\frac{\partial}{\partial x} \approx D_x = \frac{1}{2h}\begin{bmatrix} -1 & 1 & & & \\ -1 & 0 & 1 & & \\ & \ddots & \ddots & \ddots & \\ & & -1 & 0 & 1 \\ & & & -1 & 1 \end{bmatrix}$$

$$\frac{\partial^2}{\partial x^2} \approx D_x^2 = \frac{1}{h^2}\begin{bmatrix} -1 & 1 & & & \\ 1 & -2 & 1 & & \\ & \ddots & \ddots & \ddots & \\ & & 1 & -2 & 1 \\ & & & 1 & -1 \end{bmatrix}.$$

Since in this project we are mainly interested in the values of state variables at $x = 0$, it is not hard to show that, due to the model's symmetry about the origin, the numerical value of any state variable computed at the point $x_1 = h/2$ is still a second-order accurate approximation to the true solution of that variable at $x = 0$.

CHAPTER 4

COMPUTATIONAL RESULTS

This chapter presents computational results of the model under various spatial and temporal settings. The values of state variables and the percent enhancement E plotted here are their corresponding values at the origin $(x,\ y) = (0,\ 0)$. The size of the flicker stimulus region S is described by the side length of a square-shaped S, the width of a slit-shaped S, or the diameter of a disk-shaped S. In other words, the size of S is equal to $2a$ where a is the half width of S introduced in Chapter 2. The frequency of the flicker stimulus is equal to $1000/P$ with units in Hz where P (ms) is the flickering period. All other parameters not mentioned in each plot below have the same values as those given in Table 1$\sim$5 in Chapter 2 except for the ephaptic coefficient α and the GABA release parameter k_G . In most plots, four different combinations of the feedback mechanisms are examined, namely, the hybrid case with both ephaptic and GABA mechanisms ($\alpha = 0.88,\ k_G = 1$), the solely ephaptic case ($\alpha = 0.88,\ k_G = 0$), the solely GABA case ($\alpha = 0,\ k_G = 1$), and the null case with neither ephaptic nor GABA mechanisms ($\alpha = 0,\ k_G = 0$).

4.1 Square S: V_H as a function of time

Fig. 4 shows the computed membrane potential V_H in the horizontal cell slab as a function of time for the model with a square-shaped flicker stimulus region S. The voltage time traces in all four cases display the "sag" and PIR properties introduced in Chapter 1. The hybrid case where both ephaptic and GABA mechanisms are present generates the percent enhancement ($E = 97.69$) that is closest to the one calculated from experimental voltage recordings under similar conditions ($E = 104$ in Fig. 1 of paper [98]). The solely ephaptic case produces an E value that is a bit less than that of the hybrid case, but is much larger than the E value generated by

the solely GABA case. The null case where both mechanisms are absent fails to generate an enhancement of the flicker response. The sum of the E values of the solely ephaptic case and the solely GABA case is clearly larger than the E value in the hybrid case, indicating that there is not a linear summation of the effects of these two feedback mechanisms.

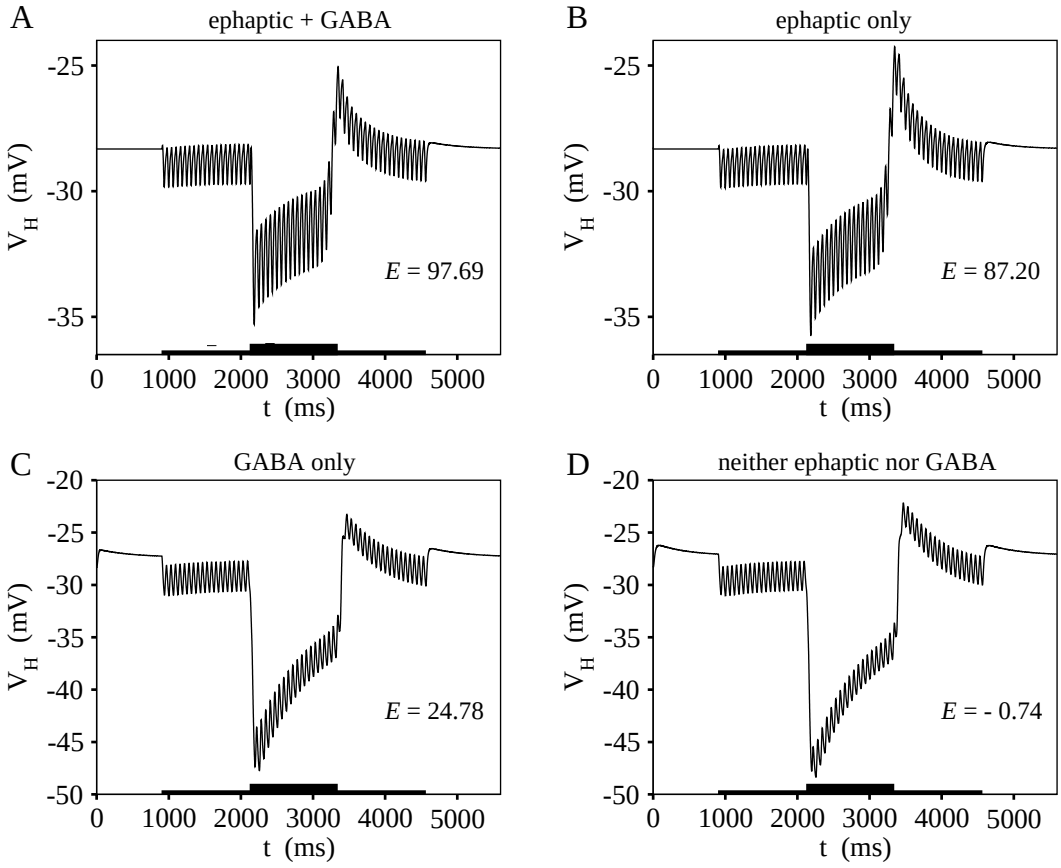

Figure 4: Horizontal cell slab membrane potential V_H as a function of time for the model with a square-shaped flicker stimulus region S. The side length of S is 250 μm, and the flicker frequency is 16 Hz. Note the different vertical scales between plots A, B and plots C, D. Along the horizontal axis of each subplot, the thin long black bar denotes the time interval when the center flicker stimulus is on, and the thick short black bar denotes the time interval when the full-field background illumination is on.

4.2 Square and slit S: E as a function of the size of S

Fig. 5 shows percent enhancement E as a function of the side length of a square-shaped flicker stimulus regions S. The simulation curve computed in the hybrid case gives the best fit with the experimental data. The curve computed in the solely ephaptic case does not fit the data as equally well as the hybrid case, but is much better than the curves in the other two cases. The solely GABA case generates a curve that is way below the experimental data, and the E values on the curve corresponding to the null case stay around zero no matter what the square width is. Fig. 6 shows similar plots for the model with a slit-shaped region S, and again the hybrid case gives the best overall fit to the data.

4.3 Square and slit S: E as a function of flicker frequency

Fig. 7 shows percent enhancement E as a function of flicker frequency for the model with a square-shaped region S. Note that the absolute values of the parameters A_{flick} and A_{bkgd} which reflect the amplitudes of the respective photocurrent I_{flick} and I_{bkgd} are increased here as compared to their values given in Table 5 because the corresponding experimental data were generated under clearly higher light intensities of the flicker stimulus and the background illumination as compared to their respective intensity levels used in producing the voltage recordings and the curve of E vs. square width [98, 88]. Both the hybrid case and the solely ephaptic case display the two-limbed feature of a slow increase in E below 20 Hz and a rapid rise in E above that frequency, but the increase of E in the former case is more prominent. The E values produced in the solely GABA case and the null case tend to decrease as the frequency increases, and they even become negative when the frequency is larger than about 20 Hz.

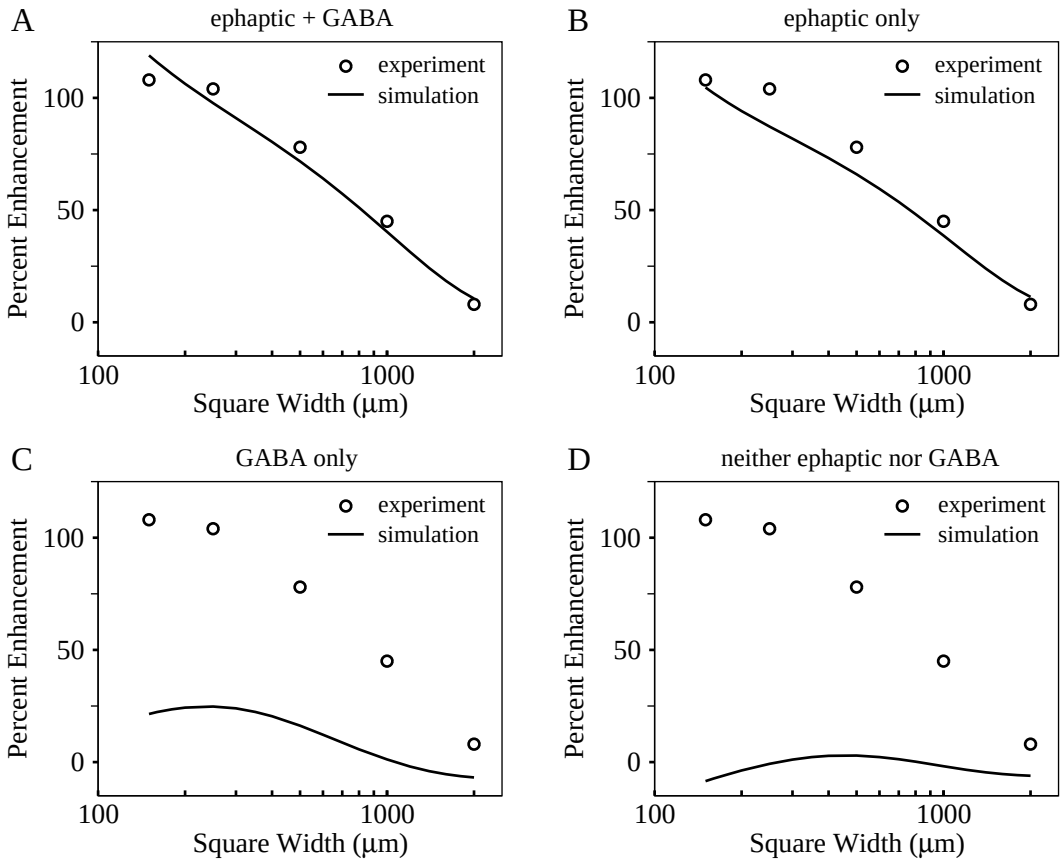

Figure 5: Percent enhancement E as a function of the side length of a square-shaped flicker stimulus region S. The solid simulation curves were generated at a flicker frequency of 16 Hz. The open circles in each subplot are experimental data taken from Fig. 5 in paper [88] for a 16 Hz square-shaped S with the flicker being at 650 nm and 6.8 log quanta $\cdot\, \mu\mathrm{m}^{-2} \cdot \mathrm{s}^{-1}$ and the background being at 423 nm and 3.4 log quanta $\cdot\, \mu\mathrm{m}^{-2} \cdot \mathrm{s}^{-1}$.

Fig. 8 shows similar plots for the model with a slit-shaped region S, and these plots demonstrate essentially the same features as those described above.

4.4 Square and slit S: background-induced phase shift

Fig. 9 shows the background-induced phase shift in the flicker response V_H for the model with a square-shaped region S. Note that the absolute value of the parameter A_{bkgd} (the hyperpolarizing amplitude of I_{bkgd}) is larger here as compared to its value given in Table 5 because the corresponding experimental data were generated under

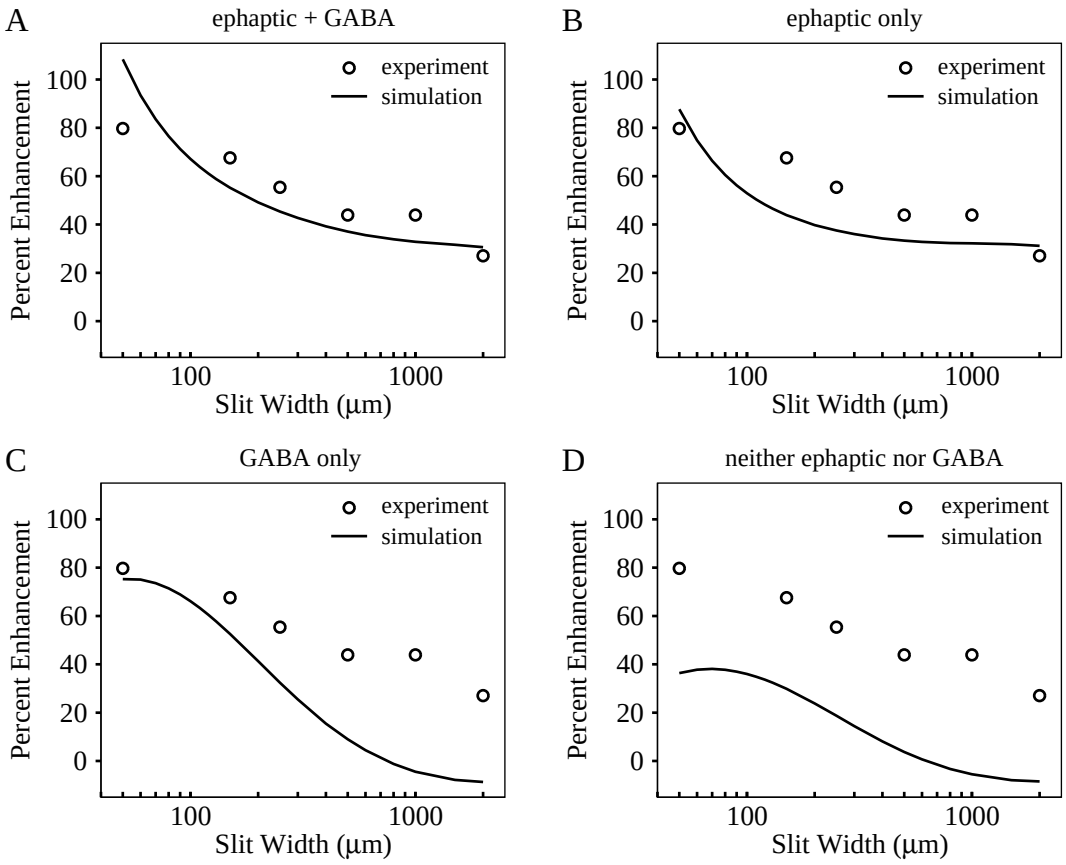

Figure 6: Percent enhancement E as a function of the width of a slit-shaped flicker stimulus region S. The solid simulation curves were generated at a flicker frequency of 20 Hz. The open circles in each subplot are experimental data taken from Fig. 6 in paper [88] for a 20 Hz slit-shaped S with the flicker being at 650 nm and 6.8 log quanta $\cdot\, \mu\mathrm{m}^{-2} \cdot \mathrm{s}^{-1}$ and the background being at 420 nm and 3.4 log quanta $\cdot\, \mu\mathrm{m}^{-2} \cdot \mathrm{s}^{-1}$.

a clearly higher light intensity of the background illumination as compared to its intensity level used in producing the voltage recordings and the curve of E vs square width (see Fig. 5 in paper [98]). Both the hybrid case and the solely ephaptic case produce background-induced phase advances of the response waveform with the amount of advance in the former being slightly larger than that in the latter, while the solely GABA case and the null case produce background-induced phase delays which are inconsistent with experimental observations [98].

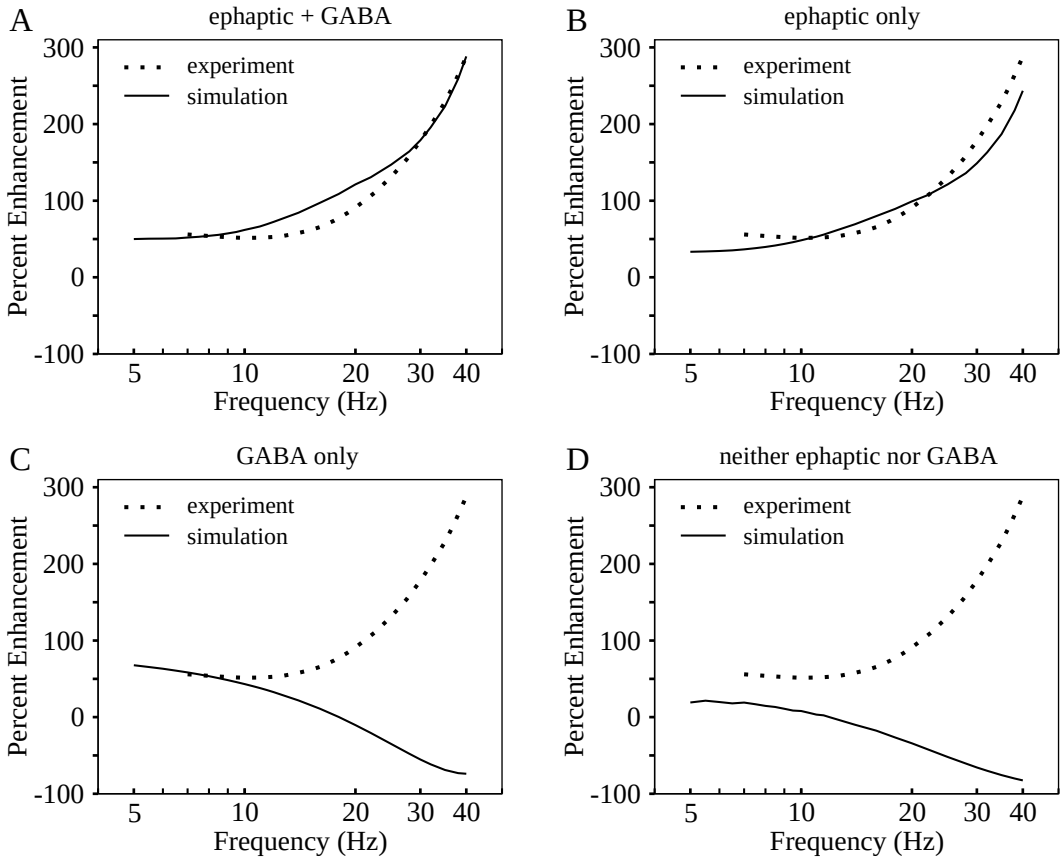

Figure 7: Percent enhancement E as a function of flicker frequency for the model with a square S. The side length of S is 150 μm. The dotted curve in each subplot consists of points taken from the cubic regression of the experimental data for a 150-μm square-shaped S with the flicker being at 650 nm and 7.3 log quanta $\cdot\, \mu\text{m}^{-2} \cdot \text{s}^{-1}$ and the background being at 420 nm and 4.4 log quanta $\cdot\, \mu\text{m}^{-2} \cdot \text{s}^{-1}$ (see Fig. 4 in paper [98]). The solid simulation curves were generated at $A_{flick} = -7.7\ \mu\text{A/cm}^2$ and $A_{bkgd} = -7.4\ \mu\text{A/cm}^2$. In C, the solid curve is a cubic regression of the simulated values, and it smoothes out some small zigzags appearing at low frequencies in the original simulation curve.

Fig. 10 shows similar plots for the model with a slit-shaped region S. Although no experimental data are available for the phase shift of flicker responses under a slit stimulus region, the simulations are consistent with those under square stimuli.

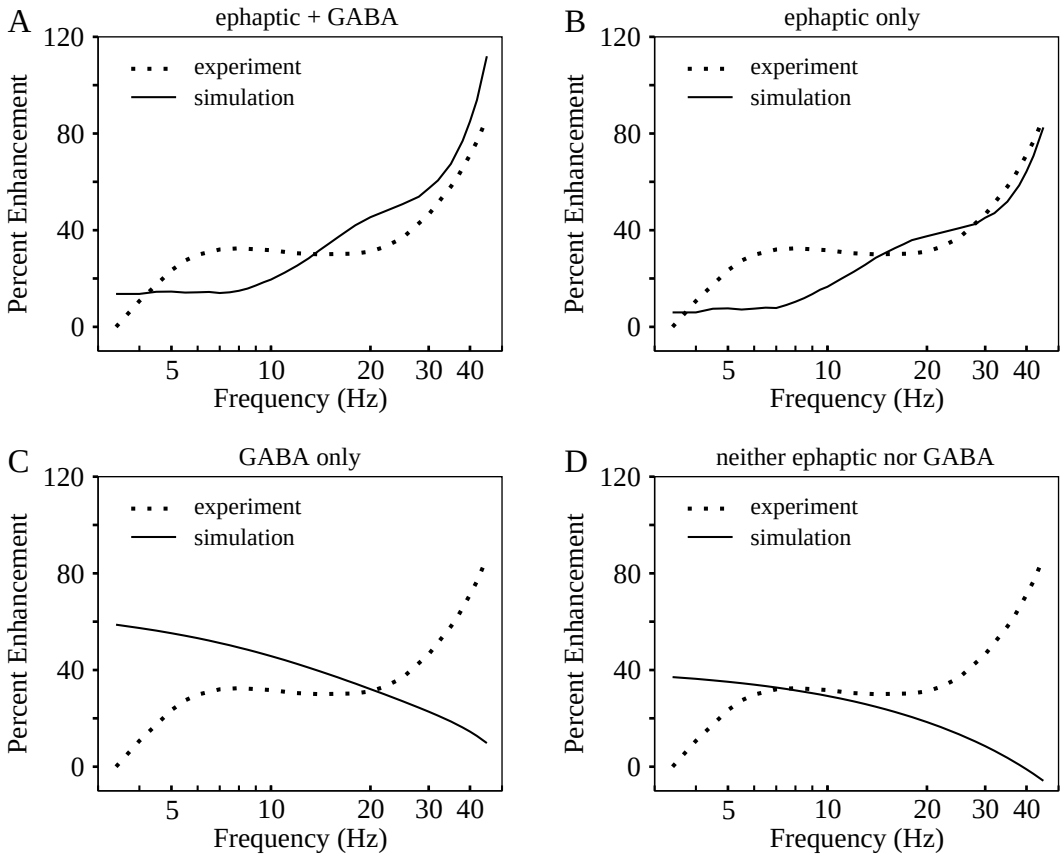

Figure 8: Percent enhancement E as a function of flicker frequency for the model with a slit S. The width of S is 250 μm. The dotted curve in each subplot consists of points taken from the cubic regression of the experimental data for a 250-μm slit-shaped S with the flicker being at 650 nm and 6.8 log quanta $\cdot\, \mu\text{m}^{-2} \cdot \text{s}^{-1}$ and the background being at 420 nm and 3.4 log quanta $\cdot\, \mu\text{m}^{-2} \cdot \text{s}^{-1}$ (see Fig. 4 in paper [98]). In C and D, the solid curves are cubic regressions of the corresponding simulated values, and they smooth out some small zigzags appearing at low frequencies in the original simulation curves.

4.5 Disk S: the curve of I_{Ca} vs. V_C

Fig. 11 plots the cone Ca^{2+} current-voltage relationships for the model with a steady disk-shaped center stimulus region both in the presence and absence of a full-field background illumination. This figure is purely a prediction since no experimental data on the cone calcium current-voltage relationship have been found for cat retina. According to the ephaptic hypothesis, background-induced hyperpolariza-

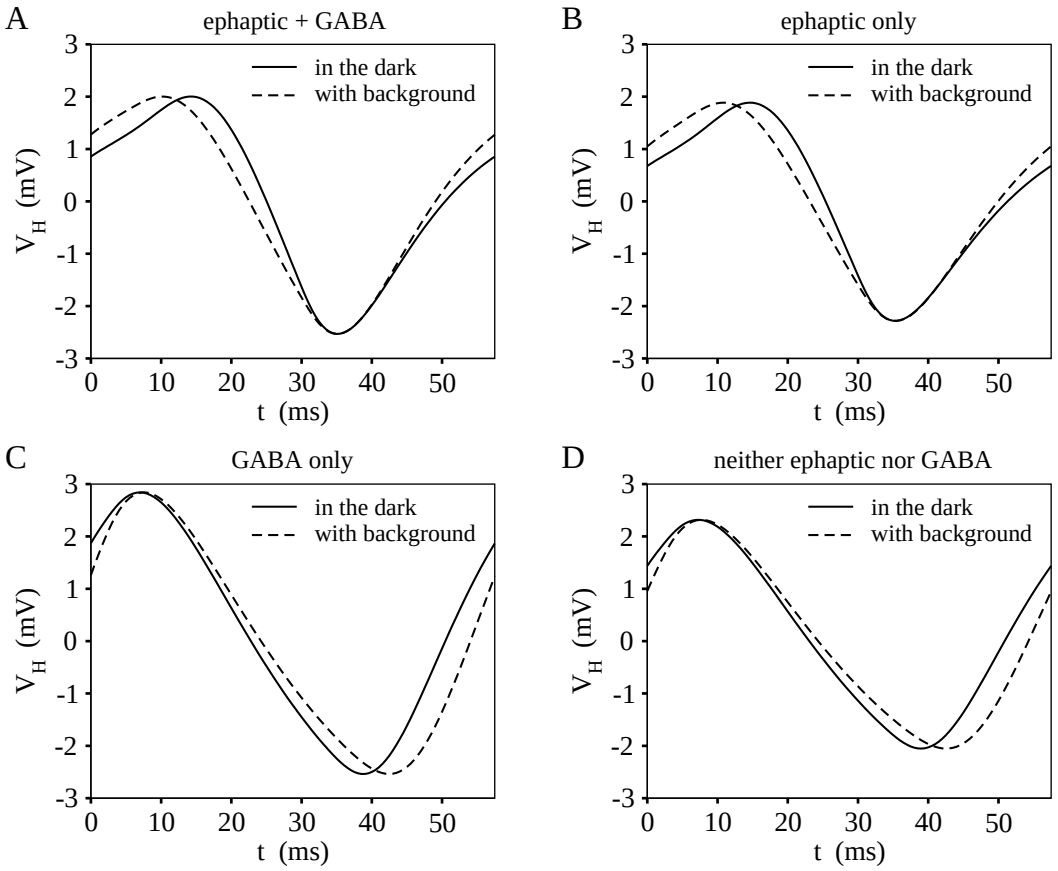

Figure 9: Background-induced phase shift in the flicker response V_H for the model with a square S. The side length of S is 424 μm, and the flicker frequency is 17.39 Hz (the corresponding flicker period $P = 57.5$ ms). All the curves were generated at $A_{bkgd} = -7.25\ \mu\text{A/cm}^2$. In each subplot, the mean single-cycle waveform of V_H before the onset of background was scaled to that during the presence of background. In addition, the two waveforms in each subplot were placed in the same time window in the sense that the difference between the starting times of the two waveforms is an integer multiple of the flicker period P.

tion of horizontal cells shifts the voltage-dependence of I_{Ca} to more negative potentials. The subplot B for the solely ephaptic case is consistent with this. The GABA hypothesis predicts that hyperpolarized horizontal cells will increase calcium channel conductance by reducing their release of the calcium channel blocking agent GABA. Thus the GABA-mediated background-induced feedback will induce an increase in peak I_{Ca}, which is shown in the subplot C for the solely GABA case.

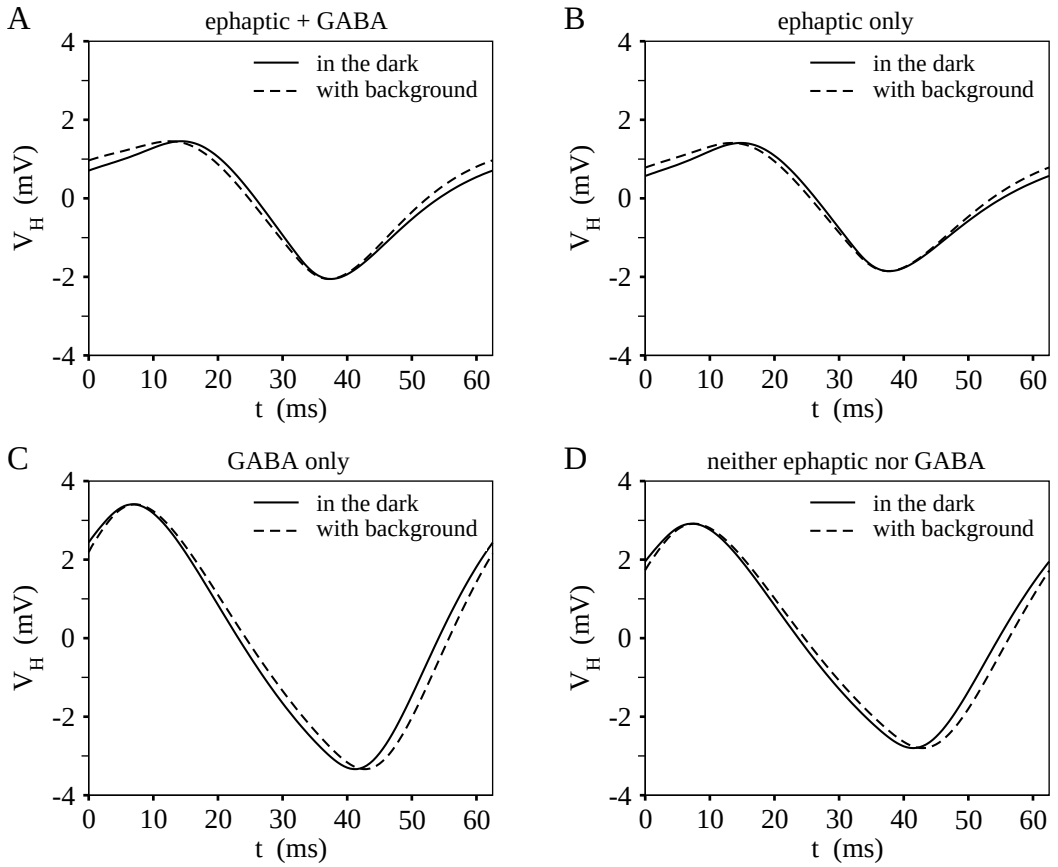

Figure 10: Background-induced phase shift in the flicker response V_H for the model with a slit S. The width of S is 250 μm, and the flicker frequency is 16 Hz (the corresponding flicker period $P = 62.5$ ms). All the curves were generated at $A_{bkgd} = -7\ \mu\text{A/cm}^2$. In each subplot, the mean single-cycle waveform of V_H before the onset of background was scaled to that during the presence of background. In addition, the two waveforms in each subplot were placed in the same time window in the sense that the difference between the starting times of the two waveforms is an integer multiple of the flicker period P.

The null case in subplot D shows no shift of the curve since no feedback mechanism is present. The hybrid case in subplot A shows both an increase in peak I_{Ca} and a negative shift for some part of the curve, clearly a combined effect of both the ephaptic and GABA mechanisms.

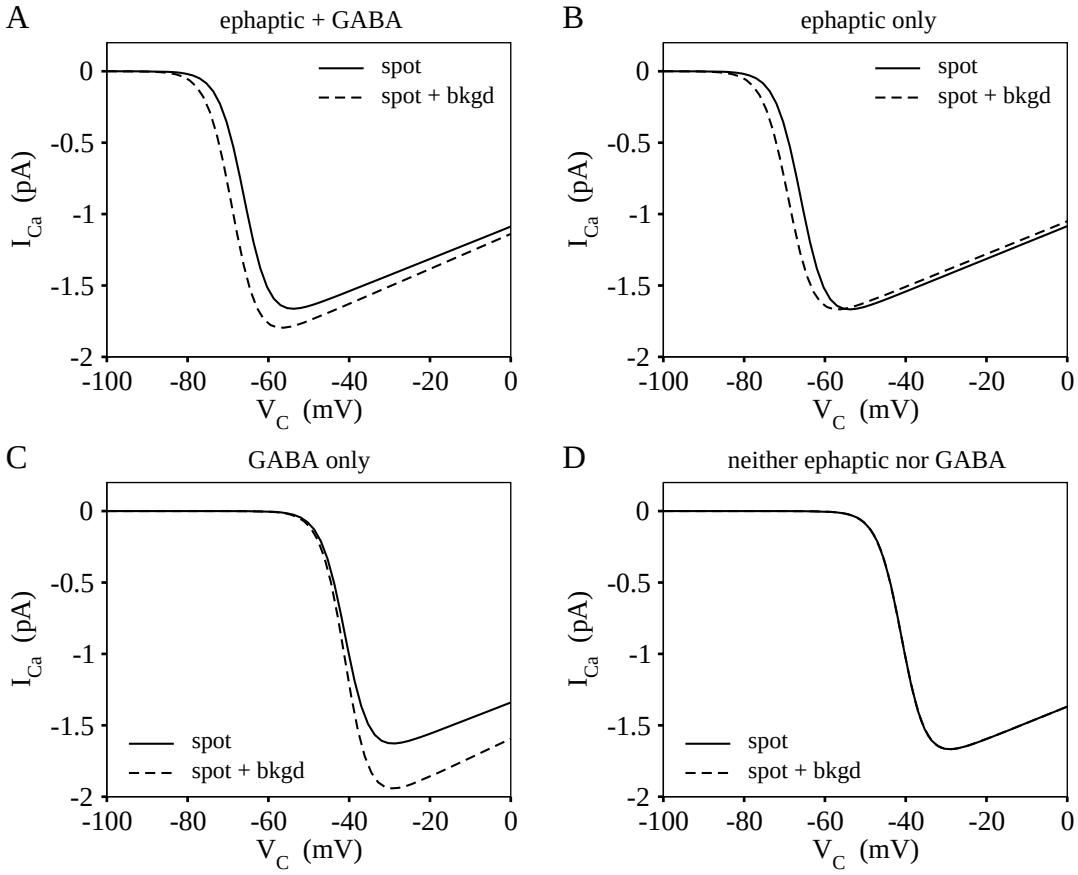

Figure 11: Shift of the voltage dependence of cone I_{Ca} by background illumination for the model with a disk S. In each subplot, the steady-state relations between cone I_{Ca} generated within a single synapse and the corresponding cone membrane potentials Vc are plotted, where the solid curve is for the model with only a non-flickering center spot of 65 μm in diameter, and the dashed curve is for the model with the center spot superimposed by a full-field background illumination.

4.6 Disk S: results are similar to those for square S

If the diameters of the regions S and Ω defined in Chapter 3 for a disk-shaped retina patch equal the corresponding side lengths of the regions S and Ω of a square-shaped retina patch (see also Fig. 2), and if the same set of parameter values are used, then, as expected, the corresponding computational results of the model with these two different spatial settings stay very close to each other. Fig. 12 is a demonstration of this feature, which shows that the change from a square retina patch with

a square stimulus region S to a corresponding disk retina patch with a disk stimulus region S does not shift the curves of E vs. frequency and E vs. the size of S too much. This is also true for the voltage time traces and the background-induced phase advances which are not shown here. Because of this feature, the computational results of the model under a disk-shaped S and those under a square-shaped S can be roughly identified. In addition, numerical solution of the model with a disk-shaped S is much faster than that with a square-shaped S since the former can be reduced to one spatial dimension as explained in Chapter 3. Therefore, to save the computational time considerably in some of the following figures, simulations generated for disk-shaped S are considered as appropriate demonstrations of model behavior and are compared with the corresponding experimental data obtained for square-shaped S whenever the data for disk-shaped S are unavailable.

4.7 The function γ is necessary for square and disk S

Fig. 13 shows the effect of the function γ defined in Eq. (2.29) on the simulation results for different shapes of stimulus regions S. Subplot B shows that whether γ is a function of the size of S or is a suitably chosen constant does not make too much difference for the model with a slit-shaped region S. However, as can be seen from subplot A, for the model with a square- or disk-shaped region S, a constant value of γ can never generate a good fit between computational results and experimental data, and defining γ as the function given in Eq. (2.29) can resolve the fitting issue.

4.8 Examples of model robustness

To test the robustness of the model behavior under changes of parameter values, the model with a disk-shaped stimulus region S is used, and two parameters are chosen to be the varying parameters. One parameter is the horizontal cell spine stem diameter D_{ss}, and the other is the sheet resistance R_s of the horizontal cell slab. D_{ss}

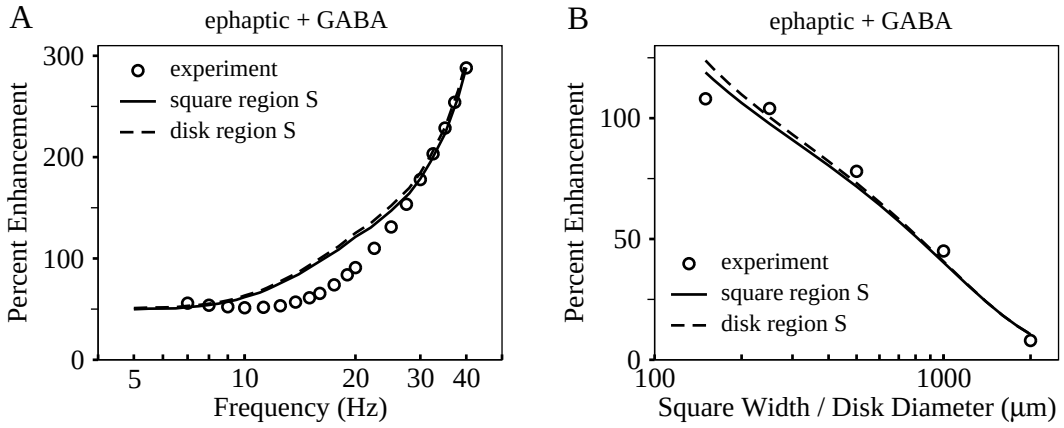

Figure 12: Comparison of results for the model with a disk-shaped S and a square-shaped S where the diameters of the regions S and Ω of the disk retina patch equal the corresponding side lengths of the regions S and Ω of the square retina patch, and all the corresponding parameter values are the same. A: Percent enhancement E as a function of flicker frequency. The diameter or the side length of S is 150 μm. The curve of open circles is the same as the dotted experimentally fitted curve for a square S of side length 150 μm described in Fig. 7. The solid and dashed simulation curves were generated at $A_{flick} = -7.7$ μA/cm^2 and $A_{bkgd} = -7.4$ μA/cm^2. B: Percent enhancement E as a function of the square width or disk diameter of the flicker stimulus region S. The solid and dashed simulation curves were generated at a flicker frequency of 16 Hz. The open circles are the same experimental data at 16 Hz for square S as described in Fig. 5.

is set to be 0.1 μm in this study and is related to the spine stem resistance R_{ss} by the formula $(4L_{ss}R_i)/(\pi D_{ss}^2)$, so a range of D_{ss} between 0.025 μm $\sim$ 1 μm corresponds to a range of R_{ss} between 1.273×10^7 Ω and 2.037×10^{10} Ω, which is consistent with the estimated range of $10^7 \sim 10^{10}$ Ω for R_{ss} [113]. Fig. 14 shows that, as D_{ss} varies within its range above, both the computed curves of E vs. frequency and E vs. the size of S remain fairly close to their corresponding experimental data.

The sheet resistance R_s controls the coupling of horizontal cells and its value is set to be 12 MΩ in this study, which is within the reported range of 7$\sim$15 MΩ for R_s [71]. In Fig. 15, R_s is varied between 1.2$\sim$120 MΩ. It can be seen that, even with this broad range of changes in R_s, the computed curves of E vs. frequency and E vs. the size of S still follow the corresponding experimental data quite well.

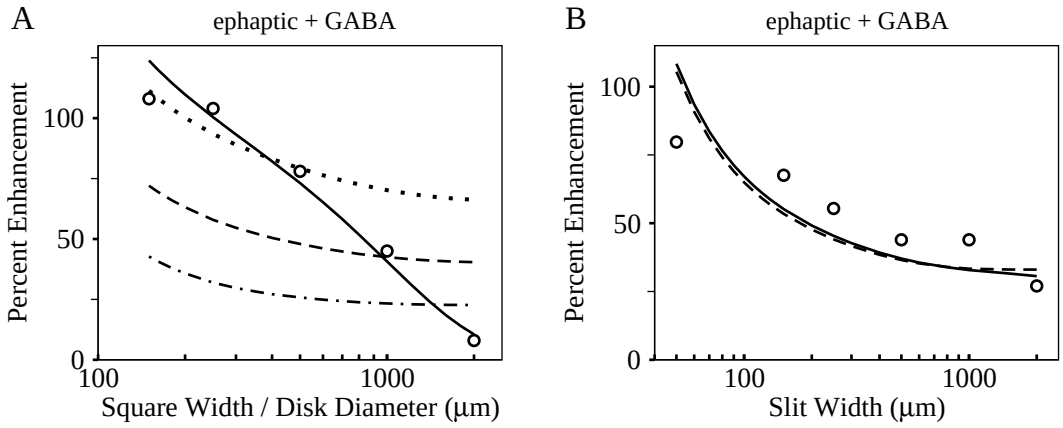

Figure 13: Effects of the function γ associated with rod desensitization defined in Eq. (2.29) on the simulation results for disk/square S and for slit S. A: Effect of γ on the model with a disk/square S. The simulation curves were generated at a flicker frequency of 16 Hz. The open circles are the same experimental data at 16 Hz for square S as described in Fig. 5. Solid curve: γ is a function of the size of S (in terms of the half width a) as given in Eq. (2.29). Dash and dot curve: $\gamma = 0.05$. Dashed curve: $\gamma = 0.1$. Dotted curve: $\gamma = 0.2$. B: Effect of γ on the model with a slit S. The simulation curves were generated at a flicker frequency of 20 Hz. The open circles are the same experimental data at 20 Hz for slit S as described in Fig. 6. Solid curve: γ is a function of the size of S (in terms of the half width a) as given in Eq. (2.29). Dashed curve: $\gamma = 0.06$.

What is not shown here is that the characteristic shape of the voltage time traces and the background-induced phase advance are also quite robust with respect to variations of the two parameters above. Thus, the model is robust under the change in spine stem diameter and hence in spine stem resistance, and is also robust with respect to the possible varying coupling strengths among horizontal cells within their slab.

4.9 Summary and conclusion

The model developed in this study displays quite robust behavior with respect to different shapes of the flicker stimulus region and reasonable variations of parameter values. In all the computational results obtained, the solely ephaptic case is able to produce simulations that fit qualitatively well with the experimental data, while

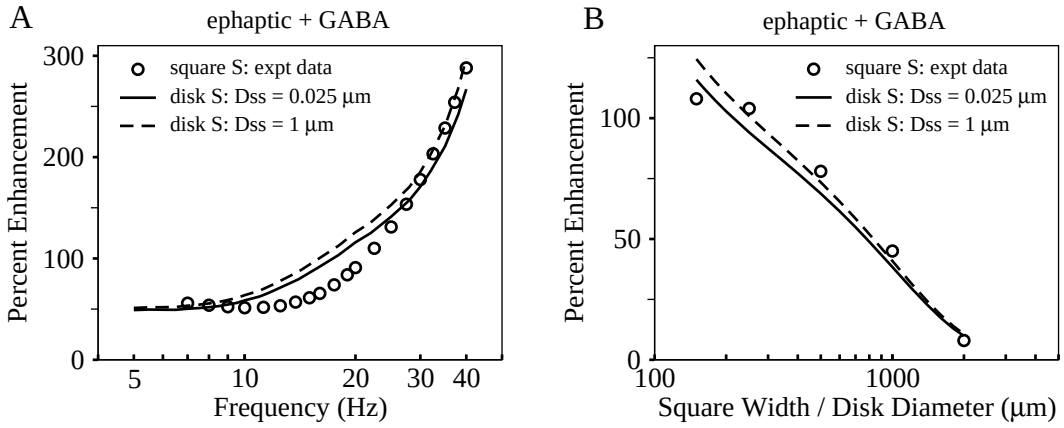

Figure 14: Robustness of the model with a disk S under the variation of horizontal cell spine stem diameter D_{ss}. A: Effect of the variation of D_{ss} on the relation between percent enhancement E and flicker frequency. The diameter of S is 150 μm. The curve of open circles are the same as the dotted experimentally fitted curve for a square S of side length 150 μm described in Fig. 7. The solid and dashed simulation curves were generated at $A_{flick} = -7.7\ \mu\text{A/cm}^2$ and $A_{bkgd} = -7.4\ \mu\text{A/cm}^2$. B: Effect of the variation of D_{ss} on the relation between percent enhancement E and the disk diameter of S. The solid and dashed simulation curves were generated at a flicker frequency of 16 Hz. The open circles are the same experimental data at 16 Hz for square S as described in Fig. 5.

the hybrid case where both ephaptic and GABA mechanisms are present is a bit better. The results generated by the solely GABA case either are not consistent with experimental observations or fail to stay close with the experimental data. These results indicate that the ephaptic mechanism is necessary in order for the model to capture the major spatial and temporal dynamics exhibited by the BIFE effect. The GABA mechanism, although contributing to the increase of percent enhancement under certain conditions, may only have some limited modulatory function.

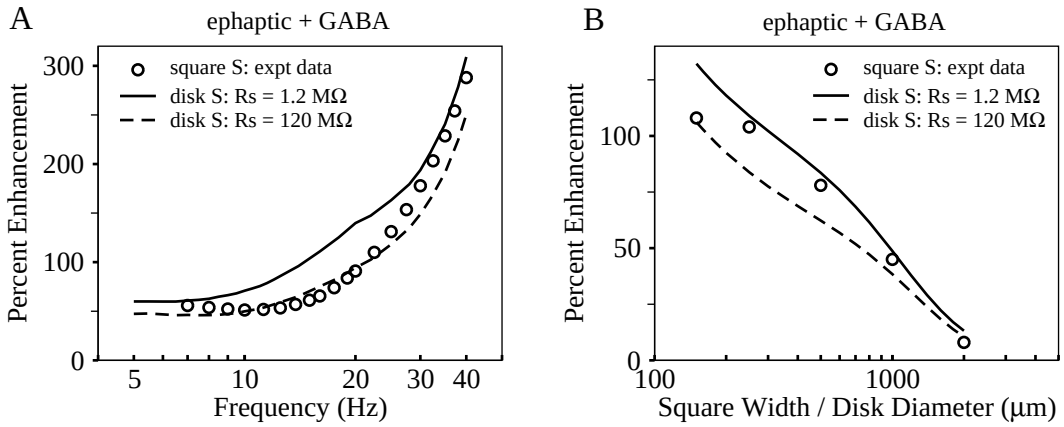

Figure 15: Robustness of the model with a disk S under the variation of the sheet resistance R_s of the horizontal cell slab. A: Effect of the variation of R_s on the relation between percent enhancement E and flicker frequency. The diameter of S is 150 μm. The curve of open circles are the same as the dotted experimentally fitted curve for a square S of side length 150 μm described in Fig. 7. The solid and dashed simulation curves were generated at $A_{flick} = -7.7$ μA/cm^2 and $A_{bkgd} = -7.4$ μA/cm^2. B: Effect of the variation of R_s on the relation between percent enhancement E and the disk diameter of S. The solid and dashed simulation curves were generated at a flicker frequency of 16 Hz. The open circles are the same experimental data at 16 Hz for square S as described in Fig. 5.

CHAPTER 5

DISCUSSION AND FUTURE DIRECTIONS

5.1 Discussion

Consider the relation between percent enhancement E and the size of the flicker stimulus region S. The experimental data shown in Fig. 5 for square-shaped S and in Fig. 6 for slit-shaped S indicate that, as the size of S decreases, E increases and gradually levels off. However, the computed E values in the hybrid case and in the solely ephaptic case tend to increase more and more rapidly as the size of S decreases (Fig. 5 A and B, and Fig. 6 A and B). This indicates that, although the model with an ephaptic feedback mechanism can produce results that have an overall good agreement with the experimental data, the model may not be appropriate for situations where the size of S is small (e.g., smaller than 100 μm). There should be some other mechanism dominant for small S that can prevent the E values from going unbounded.

Upon the onset of background illumination, the cone Ca^{2+} current-voltage curve measured experimentally in gold fish and some other species does not have a visible shift in its rightmost branch (i.e., in the more depolarized holding potentials) [41, 135], which looks different from those computed in this study and shown in Fig. 11. But there is one thing in Fig. 11 that is worth noticing. In subplot B, $K_G = 0$ and the rightmost branch of the curve is shifted a little bit up by the background illumination, while in subplot A, $K_G = 1$ and the rightmost branch of the current-voltage curve is dragged down by the background illumination. Thus we can expect that with an appropriate value of K_G between 0 and 1 (maybe just slightly positive), the background-induced vertical shift of the rightmost branch of the curve can be minimized so that the shift there is almost invisible. Now the

resulting overall shift displayed by the computed current-voltage relationship will be similar to those observed in experiments. However, in this computed shift, the GABA mechanism has some small yet nonzero effect since K_G is positive, while the shift generated experimentally was claimed to be GABA-independent since the measurements were carried out in the presence of a high concentration of picrotoxin, which is a $GABA_A$ receptor antagonist and can block all $GABA_A$-receptor-mediated feedback responses [135]. One possible explanation for such a seeming disagreement is as follows. There are suggestions that the GABAergic feedback mechanism examined in this study (i.e., the first version of the GABA hypothesis introduced in Chapter 1) is mediated by $GABA_B$ receptors [27, 73, 87, 100, 135] on which picrotoxin has no effect [103]. This $GABA_B$-receptor-mediated feedback, albeit small, might indeed survive in those experimental conditions and could be used to adjust the computed shift of the current-voltage curve into a shape similar to the experimental one if the feedback strength is appropriate (as reflected by the value of K_G).

5.2 Future Directions

Rods are not modeled explicitly in this study. It might be desirable to incorporate rods into the model and also take into account the rod-rod, cone-cone electrical couplings in addition to the rod-cone couplings as introduced in Chapter 1. The study of such a modified model might provide some judgement on the expression of the rod-desensitization-associated function γ defined in Eq. (2.29).

This study assumes uniform distribution of horizontal cell spines. However, the distribution of cones in an actual retina is non-uniform with its density in the fovea being the highest and decreasing rapidly towards the peripheral retina [10]. Since A-type horizontal cells only make synaptic contacts with cones, this implies that the distribution of horizontal cell dendritic spines will also be non-uniform. It

is interesting to see if such a modification will affect the light responses of cones and horizontal cells, and if it can improve the agreement between simulation and experiment.

This study assumes that the length constant of the horizontal cell slab remains unchanged. However, there are reports showing that the length constant is dynamic and depends on factors such as light intensity and endogenous dopamine concentration [11, 50, 94, 136, 146]. Incorporating such mechanisms into the model could improve the accuracy of model predictions and make it more flexible to various spatial and temporal settings.

Formulation of a transfer function between light intensity and photocurrent density may be desirable. This will make direct connections between flicker stimulus intensity and I_{flick}, and also between the intensity of background illumination and I_{bkgd}. Thus a direct study of the influence of background intensity on percent enhancement will be possible. This will also allow a more accurate description of photoreceptor light responses.

The mathematical model and computational code developed in this study provides a basis for the theoretical investigation of the response of the outer retina to various forms of light stimuli such as a moving non-flickering stimulus, and provides the opportunity for comparing the light response to such a stimulus with that to a stationary flickering stimulus.

REFERENCES

[1] P. K. Ahnelt, C. Keri, and H. Kolb. Identification of pedicles of putative blue sensitive cones in human and primate retina. *J. Comp. Neurol.*, 293:39–53, 1990.

[2] G. B. Arden and T. E. Frumkes. Stimulation of rods can increase cone flicker ERGs in man. *Vision Res.*, 26:711–721, 1986.

[3] G. S. Ayoub and D. M. K. Lam. The content and release of endogenous GABA in isolated horizontal cells of the goldfish retina. *Vision Res.*, 25:1187–1193, 1985.

[4] N. Babai and W. B. Thoreson. Horizontal cell feedback regulates calcium currents and intracellular calcium levels in rod photoreceptors of salamander and mouse retina. *J. Physiol.*, 587:2353–2364, 2009.

[5] S. M. Baer and J. Rinzel. Propogation of dendritic spikes mediated by excitable spikes: A continuum theory. *J. Neurophysiol.*, 65:874–890, 1991.

[6] S. Barnes and Q. Bui. Modulation of calcium-activated chloride current via pH-induced changes of calcium channel properties in cone photoreceptors. *J. Neurosci.*, 11:4015–4023, 1991.

[7] S. Barnes and M. C. Deschenes. Contribution of Ca and Ca-activated Cl channels to regenerative depolarization and membrane bistability of cone photoreceptors. *J. Neurophysiol.*, 68:745–755, 1992.

[8] S. Barnes, V. Merchant, and F. Mahmud. Modulation of transmission gain by protons at the photoreceptor output synapse. *Proc. Natl. Acad. Sci. USA*, 90:10081–10085, 1993.

[9] B. B. Bean. Neurotransmitter inhibition of neuronal calcium currents by changes in channel voltage dependence. *Nature*, 340:153–156, 1989.

[10] M. F. Bear, B. W. Connors, and M. A. Paradiso. *Neuroscience: Exploring the Brain. 3rd Ed.* Lippincott Williams & Wilkins, New York, 2007.

[11] J. Benda, R. Bock, P. Rujan, and J. Ammermüller. Asymmetrical dynamics of voltage spread in retinal horizontal cell networks. *Vis. Neurosci.*, 18:835–848, 2001.

[12] M. Bouvier, M. Szatkowski, A. Amato, and D. Attwell. The glial cell glutamate uptake carrier countertransports pH-changing anions. *Nature*, 360:471–474, 1992.

[13] D. A. Burkhardt. Synaptic feedback, depolarization, and color opponency in cone photoreceptors. *Vis. Neurosci.*, 10:981–989, 1993.

[14] D. A. Burkhardt, S. Zhang, and J. Gottesman. Prolonged depolarization in rods in situ. *Vis. Neurosci.*, 6:607–614, 1991.

[15] A. L. Byzov and T. M. Shura-Bura. Electrical feedback mechanism in the processing of signals in the outer plexiform layer of the retina. *Vision Res.*, 26:33–44, 1986.

[16] L. Cadetti and W. B. Thoreson. Feedback effects of horizontal cell membrane potential on cone calcium currents studied with simultaneous recordings. *J. Neurophysiol.*, 95:1992–1995, 2006.

[17] X. H. Chen, I. Bezprozvanny, and R. W. Tsien. Molecular basis of proton block of L-type Ca^{2+} channels. *J. Gen. Physiol.*, 108:363–374, 1996.

[18] M.-H. Chun, U. Grünert, P. R. Martin, and H. Wässle. The synaptic complex of cones in the fovea and in the periphery of the macaque monkey retina. *Vision Res.*, 36:3383–3395, 1996.

[19] M.-H. Chun and H. Wässle. GABA-like immunoreactivity in the cat retina: Electron microscopy. *J. Comp. Neurol.*, 279:55–67, 1989.

[20] V. Connaughton. In H. Kolb, R. Nelson, E. Fernandez, and B. Jones, editors, WEBVISION*: The Organization of the Retina and Visual System*, chapter Glutamate and glutamate receptors in the vertebrate retina. *http://webvision.med.utah.edu/*, 2012.

[21] C. M. Davenport, P. B. Detwiler, and D. M. Dacey. Effects of pH buffering on horizontal and ganglion cell light responses in primate retina: evidence for the proton hypothesis of surround formation. *J. Neurosci.*, 28:456–464, 2008.

[22] R. A. Deisz and H. D. Lux. γ-aminobutyric acid-induced depression of calcium currents of chick sensory neurons. *Neurosci. Lett.*, 56:205–210, 1985.

[23] S. H. DeVries. Exocytosed protons feedback to suppress the Ca^{2+} current in mammalian cone photoreceptors. *Neuron*, 32:1107–1117, 2001.

[24] S. H. DeVries, X. Qi, R. Smith, W. Makous, and P. Sterling. Electrical coupling between mammalian cones. *Curr. Biol.*, 12:1900–1907, 2002.

[25] A. V. Dmitriev and S. C. Mangel. Electrical feedback in the cone pedicle: A computational analysis. *J. Neurophysiol.*, 95:1419–1427, 2006.

[26] E. Dodt. Cone electroretinography by flicker. *Nature*, 168:738, 1951.

[27] A. C. Dolphin and R. H. Scott. Inhibition of calcium currents in cultured rat dorsal root ganglion neurons by (-)-baclofen. *Br. J. Pharmac.*, 88:213–220, 1986.

[28] K. Dunlap and G. D. Fischbach. Neurotransmitters decrease the calcium component of sensory neuron action potentials. *Nature*, 276:837–839, 1978.

[29] K. Dunlap and G. D. Fischbach. Neurotransmitters decrease the calcium conductance activated by depolarization of embryonic chick sensory neurons. *J. Physiol.*, 317:519–535, 1981.

[30] I. Fahrenfort, T. Sjoerdsma, H. Ripps, and M. Kamermans. Cobalt ions inhibit negative feedback in the outer retina by blocking hemichannels on the horizontal cells. *Vis. Neurosci.*, 21:501–511, 2004.

[31] I. Fahrenfort, M. Steijaert, T. Sjoerdsma, E. Vickers, H. Ripps, J. van Asselt, D. Endeman, J. Klooster, R. Numan, H. ten Eikelder, H. von Gersdorff, and M. Kamermans. Hemichannel-mediated and pH-based feedback from horizontal cells to cones in the vertebrate retina. *PLoS One*, 4:e6090, 2009.

[32] R. Fatechand. Attenuation of the frog's cone system during rapid dark adaptation. *Vision Res.*, 19:279–286, 1979.

[33] T. E. Frumkes and T. Eysteinsson. Suppressive rod-cone interaction in distal vertebrate retina: intracellular records from *Xenopus* and *Necturus*. *J. Neurophysiol.*, 57:1361–1382, 1987.

[34] T. E. Frumkes and T. Eysteinsson. The cellular basis for suppressive rod-cone interaction. *Visual Neurosci.*, 1:263–273, 1988.

[35] Y. Fu. In H. Kolb, R. Nelson, E. Fernandez, and B. Jones, editors, WEBVISION*: The Organization of the Retina and Visual System*, chapter Phototransduction in rods and cones. *http://webvision.med.utah.edu/*, 2012.

[36] H. M. Gerschenfeld, M. Piccolino, and J. Neyton. Feed-back modulation of cone synapses by L-horizontal cells of turtle retina. *J. Exp. Biol.*, 89:177–192, 1980.

[37] S. H. Goldberg, T. E. Frumkes, and R. W. Nygaard. Inhibitory influence of unstimulated rods in the human retina: evidence provided by examining cone flicker. *Science*, 221:180–182, 1983.

[38] C. Y. Guo, A. A. Hirano, S. L. Stella, M. Bitzer, and N. C. Brecha. Guinea pig horizontal cells express GABA, the GABA-synthesizing enzyme GAD(65), and the GABA vesicular transporter. *J. Comp. Neurol.*, 518:1647–1669, 2010.

[39] W. A. Hagins, R. D. Penn, and S. Yoshikami. Dark current and photocurrent in retinal rods. *Biophys. J.*, 10:380–412, 1970.

[40] R. Heidelberger and G. Matthews. Inhibition of calcium influx and calcium current by γ-aminobutyric acid in single synaptic terminals. *Proc. Natl. Acad. Sci. USA*, 88:7135–7139, 1991.

[41] H. Hirasawa and A. Kaneko. pH changes in the invaginating synaptic cleft mediate feedback from horizontal cells to cone photoreceptors by modulating Ca^{2+} channels. *J. Gen. Physiol.*, 122:657–671, 2003.

[42] S. Hombach, U. Janssen-Bienhold, G. Söhl, T. Schubert, H. Büssow, T. Ott, R. Weiler, and K. Willecke. Functional expression of connexin57 in horizontal cells of the mouse retina. *Eur. J. Neurosci.*, 19:2633–2640, 2004.

[43] D. H. Hood. Suppression of the frog's cone system in the dark. *Vision Res.*, 12:889–908, 1972.

[44] Klaassen L. J., Sun Z., Steijaert M. N., Bolte P., Fahrenfort I., Sjoerdsma T., Klooster J., Claassen Y., Shields C. R., Eikelder H. M. M. T., Janssen-Bienhold U., Zoidl G., McMahon D. G., and Kamermans M. Synaptic transmission from horizontal cells to cones is impaired by loss of connexin hemichannels. *PLoS Biology*, 9:e1001107, 2011.

[45] J. J. B. Jack, D. Noble, and R. W. Tsien. *Electric Current Flow in Excitable Cells*. Oxford, Clarendon, 1975.

[46] U. Janssen-Bienhold, K. Schultz, A. Gellhaus, P. Schmidt, J. Ammermuller, and R. Weiler. Identification and localization of connexin26 within the photoreceptor-horizontal cell synaptic complex. *Vis. Neurosci.*, 18:169–178, 2001.

[47] M. A. Johnson and N. Vardi. Regional differences in GABA and GAD immunoreactivity in rabbit horizontal cells. *Vis. Neurosci.*, 15:743–753, 1998.

[48] M. Kamermans and I. Fahrenfort. Ephaptic interactions within a chemical synapse: Hemichannel-mediated ephaptic inhibition in the retina. *Curr. Opin. Neurobiol.*, 14:531–541, 2004.

[49] M. Kamermans, I. Fahrenfort, K. Schultz, U. Janssen-Bienhold, T. Sjoerdsma, and R. Weiler. Hemichannel-mediated inhibition in the outer retina. *Science*, 292:1178–1180, 2001.

[50] M. Kamermans, J. Haak, J. B. A. Habraken, and H. Spekreijse. The size of the horizontal receptive fields adapts to the stimulus in the light adapted goldfish retina. *Vision Res.*, 24:4105–4120, 1996.

[51] M. Kamermans, D. Kraaij, and H. Spekreijse. The dynamic characteristics of the feedback signal from horizontal cells to cones in the goldfish retina. *J. Physiol.*, 534:489–500, 2001.

[52] M. Kamermans and H. Spekreijse. The feedback pathway from horizontal cells to cones: A mini review with a look ahead. *Vision Res.*, 39:2449–2468, 1999.

[53] A. Kaneko and M. Tachibana. Retinal bipolar cells with double colour-opponent receptive fields. *Nature*, 293:220–223, 1981.

[54] A. Kaneko and M. Tachibana. Effects of γ-aminobutyric acid on isolated cone photoreceptors of the turtle retina. *J. Physiol.*, 373:443–461, 1986.

[55] U. Klockner and G. Isenberg. Calcium channel current of vascular smooth muscle cells: extracellular protons modulate gating and single channel conductance. *J. Gen. Physiol.*, 103:665–678, 1994.

[56] C. Koch. *Biophysics of Computation: Information Processing in Single Neurons*. Oxford University Press, Inc., New York, 1999.

[57] H. Kolb. The connections between horizontal cells and photoreceptors in the retina of the cat: Electron microscopy of Golgi preparations. *J. Comp. Neurol.*, 155:1–14, 1974.

[58] H. Kolb. The organization of the outer plexiform layer in the retina of the cat: Electron microscopic observations. *J. Neurocytol.*, 6:131–153, 1977.

[59] H. Kolb. In H. Kolb, R. Nelson, E. Fernandez, and B. Jones, editors, WEBVISION*: The Organization of the Retina and Visual System*, chapter Outer plexiform layer. *http://webvision.med.utah.edu/*, 2012.

[60] H. Kolb. In H. Kolb, R. Nelson, E. Fernandez, and B. Jones, editors, WEBVISION*: The Organization of the Retina and Visual System*, chapter Photoreceptors. *http://webvision.med.utah.edu/*, 2012.

[61] H. Kolb. In H. Kolb, R. Nelson, E. Fernandez, and B. Jones, editors, WEBVISION*: The Organization of the Retina and Visual System*, chapter Part IV: Neurotransmitters in the retina. *http://webvision.med.utah.edu/*, 2012.

[62] D. A. Kraaij, H. Spekreijse, and M. Kamermans. The nature of surround-induced depolarizing responses in goldfish cones. *J. Gen. Physiol.*, 115:3–15, 2000.

[63] D. A. Kraaij, H. Spekreijse, and M. Kamermans. The open- and closed-loop gain-characteristics of the cone/horizontal cell synapse in goldfish retina. *J. Neurophysiol.*, 84:1256–1265, 2000.

[64] D. S. Krafte and R. S. Kass. Hydrogen ion modulation of Ca channel current in cardiac ventricular cells. Evidence for multiple mechanisms. *J. Gen. Physiol.*, 91:641–657, 1988.

[65] M. A. Kreitzer, L. P. Collis, A. J. A. Molina, P. J. S. Smith, and R. P. Malchow. Modulation of extracellular proton fluxes from retinal horizontal cells of the catfish by depolarization and glutamate. *J. Gen. Physiol.*, 130:169–182, 2007.

[66] D. M. K. Lam, E. M. Lasater, and K.-I. Naka. γ-aminobutyric acid: A neurotransmitter candidate for cone horizontal cells of the catfish retina. *Proc. Natl. Acad. Sci. USA*, 75:6310–6313, 1978.

[67] D. M. K. Lam, Y. Y. T. Su, L. Swain, R. E. Marc, C. Brandon, and J.-Y. Wu. Immunocytochemical localisation of L-glutamic acid decarboxylase in the goldfish retina. *Nature*, 278:565–567, 1979.

[68] T. D. Lamb. Spatial properties of horizontal cell responses in the turtle retina. *J. Physiol.*, 263:239–255, 1976.

[69] A. Lasansky. Synaptic action mediating cone responses to annular illumination in the retina of the larval tiger salamander. *J. Physiol.*, 310:205–214, 1981.

[70] E. M. Lasater. Membrane properties of distal retinal neurons. *Prog. Retin. Res.*, 11:215–246, 1991.

[71] E. M. Lasater and J. E. Dowling. In M. V. L. Bennett and D. C. Spray, editors, *Gap* J*unctions*, chapter Electrical coupling between pairs of isolated fish horizontal cells is modulated by dopamine and cAMP, pages 393–404. Cold Spring Harbor Laboratory, Cold Spring Harbor, 1985.

[72] R. J. LeVeque. *Finite Difference Methods for Ordinary and Partial Differential Equations: Steady-State and Time-Dependent Problems*. Society for Industrial and Applied Mathematics, Philadelphia, 2007.

[73] M. Y. Lipin, R. G. Smith, and W. R. Taylor. Maximizing contrast resolution in the outer retina of mammals. *Biol Cybern*, 103:57–77, 2010.

[74] S. Löhrke and H.-D. Hofmann. Voltage-gated currents of rabbit a- and b-type horizontal cells in retinal monolayer cultures. *Vis. Neurosci.*, 11:369–378, 1994.

[75] D. I. A. MacLeod. Rods cancel cones in flicker. *Nature*, 235:173–174, 1972.

[76] S. C. Mangel, M. Ariel, and J. E. Dowling. Effects of acidic amino acid antagonists upon the spectral properties of carp horizontal cells: circuitry of the outer retina. *J. Neurosci.*, 5:2839–2850, 1985.

[77] R. E. Marc. Structural organization of GABAergic circuitry in ectotherm retinas. *Prog. Brain. Res.*, 90:61–92, 1992.

[78] R. E. Marc, W. K. Stell, D. Bok, and D. M. K. Lam. GABA-ergic pathways in the goldfish retina. *J. Comp. Neurol.*, 182:221–245, 1978.

[79] C. Marchetti, E. Carbone, and H. D. Lux. Effects of dopamine and noradrenaline on Ca channels of cultured sensory and sympathetic neurons of chick. *Pflug. Arch. Eur. J. Phy.*, 406:104–111, 1986.

[80] A. V. Maricq and J. I. Korenbrot. Calcium and calcium-dependent chloride currents generate action potentials in solitary cone photoreceptors. *Neuron*, 1:503–515, 1988.

[81] The MathWorks™. MATLAB® R2011a documentation: Solve initial value problems for ordinary differential equations. *http://www.mathworks.com/help/techdoc/ref/ode23.html*, 2011.

[82] M. Murakami, Y. Shimoda, K. Nakatani, E. I. Miyachi, and S. I. Watanabe. GABA-mediated negative feedback and color opponency in carp retina. *Jpn. J. Physiol.*, 32:927–935, 1982.

[83] M. Murakami, Y. Shimoda, K. Nakatani, E. I. Miyachi, and S. I. Watanabe. GABA-mediated negative feedback from horizontal cells to cones in carp retina. *Jpn. J. Physiol.*, 32:911–926, 1982.

[84] M. Nachman-Clewner, R. St. Jules, and E. Townes-Anderson. L-type calcium channels in the photoreceptor ribbon synapse: localization and role in plasticity. *J. Comp. Neurol.*, 415:1–16, 1999.

[85] K. I. Naka and W. A. H. Rushton. The generation and spread of S-potentials in fish (C*yprinidae*). *J. Physiol.*, 192:437–461, 1967.

[86] R. Nelson. Cat cones have rod input: A comparison of the response properties of cones and horizontal cell bodies in the retina of the cat. *J. Comp. Neurol.*, 172:109–135, 1977.

[87] R. Nelson and V. Connaughton. In H. Kolb, R. Nelson, E. Fernandez, and B. Jones, editors, WEBVISION*: The Organization of the Retina and Visual System*, chapter Bipolar cell pathways in the vertebrate retina. *http://webvision.med.utah.edu/*, 2012.

[88] R. Nelson, R. Pflug, and S. M. Baer. Background-induced flicker enhancement in cat retinal horizontal cells. II. spatial properties. *J. Neurophysiol.*, 64:326–340, 1990.

[89] B. II. Oakley and R. Wen. Extracellular pH in the isolated retina of the toad in darkness and during illumination. *J. Physiol.*, 419:353–378, 1989.

[90] J. J. O'Brien, W. Li, F. Pan, J. Keung, J. O'Brien, and S. C. Massey. Coupling between A-type horizontal cells is mediated by Connexin 50 gap junctions in the rabbit retina. *J. Neurosci.*, 26:11624–11636, 2006.

[91] P. M. O'Bryan. Properties of the depolarizing synaptic potential evoked peripheral illumination in cones of the turtle retina. *J. Physiol.*, 235:207–223, 1973.

[92] B. Pattnaik, A. Jellali, J. Sahel, H. Dreyfus, and S. Picaud. GABA(C) receptors are localized with microtubule-associated protein 1B in mammalian cone photoreceptors. *J. Neurosci.*, 20:6789–6796, 2000.

[93] I. Perlman. In H. Kolb, R. Nelson, E. Fernandez, and B. Jones, editors, WEBVISION*: The Organization of the Retina and Visual System*, chapter The electroretinogram: ERG. *http://webvision.med.utah.edu/*, 2012.

[94] I. Perlman and J. Ammermüller. Receptive-field size of L1 horizontal cells in the turtle retina: Effects of dopamine and background light. *J. Neurophysiol.*, 72:2786–2795, 1994.

[95] I. Perlman, H. Kolb, and R. Nelson. In H. Kolb, R. Nelson, E. Fernandez, and B. Jones, editors, WEBVISION*: The Organization of the Retina and Visual System*, chapter S-potentials and horizontal cells. *http://webvision.med.utah.edu/*, 2012.

[96] I. Perlman and R. A. Normann. Light adaptation and sensitivity controlling mechanisms in vertebrate photoreceptors. *Prog. Retin. Eye Res.*, 17:523–563, 1998.

[97] C. Pfeiffer-Linn and E. M. Lasater. Dopamine modulates in a differential fashion T- and L-type calcium currents in bass retinal horizontal cells. *J. Gen. Physiol.*, 102:277–294, 1993.

[98] R. Pflug, R. Nelson, and P. K. Ahnelt. Background-induced flicker enhancement in cat retinal horizontal cells. I. temporal and spectral properties. *J. Neurophysiol.*, 64:313–325, 1990.

[99] S. Picaud, B. Pattnaik, D. Hicks, V. Forster, V. Fontaine, J. Sahel, and H. Dreyfus. GABA(A) and GABA(C) receptors in adult porcine cones: evidence from a photoreceptor-glia co-culture model. *J. Physiol.*, 513:33–42, 1998.

[100] M. Piccolino. The feedback synapse from horizontal cells to cone photoreceptors in the vertebrate retina. *Prog. Retin. Eye Res.*, 14:141–196, 1995.

[101] M. Pottek, K. Schultz, U. Janssen-Bienhold, and R. Weiler. Physiological and anatomical evidence for an involvement of Connexin26 in the negative feedback loop between horizontal cells and cones in turtle. *J. Comp. Neurol.*, 466:468–477, 2003.

[102] B. Prod'hom, D. Pietrobon, and P. Hess. Direct measurement of proton transfer rates to a group controlling the dihydropyridine-sensitive Ca^{2+} channel. *Nature*, 329:243–246, 1987.

[103] H. Qian. In H. Kolb, R. Nelson, E. Fernandez, and B. Jones, editors, WEBVISION*: The Organization of the Retina and Visual System*, chapter GABAc receptors in the vertebrate retina. *http://webvision.med.utah.edu/*, 2012.

[104] E. Raviola and N. B. Gilula. Gap junctions between photoreceptor cells in the vertebrate retina. *Proc. Nat. Acad. Sci. USA*, 70:1677–1681, 1973.

[105] P. V. Sarthy and M. Fu. Localization of L-glutamic acid decarboxylase mRNA in cat retinal horizontal cells by in situ hybridization. *J. Comp. Neurol.*, 288:593–600, 1989.

[106] Y. Schmitz and P. Witkovsky. Dependence of photoreceptor glutamate release on a dihydropyridine-sensitive calcium channel. *J. Neurosci.*, 78:1209–1216, 1997.

[107] D. M. Schneeweis and J. L. Schnapf. Photovoltage of rods and cones in the macaque retina. *Science*, 268:1053–1056, 1995.

[108] T. Schubert, R. Weiler, and A. Feigenspan. Intracellular calcium is regulated by different pathways in horizontal cells of the mouse retina. *J. Neurophysiol.*, 96:1278–1292, 2006.

[109] E. A. Schwartz. Rod-rod interaction in the retina of the turtle. *J. Physiol.*, 246:617–638, 1975.

[110] E. A. Schwartz. Calcium-independent release of GABA from isolated horizontal cells of the toad retina. *J. Physiol.*, 323:211–227, 1982.

[111] E. A. Schwartz. Depolarization without calcium can release gamma-aminobutyric acid from a retinal neuron. *Science*, 238:35–355, 1987.

[112] E. A. Schwartz. Transport-mediated synapses in the retina. *Physiol. Rev.*, 82:875–891, 2002.

[113] I. Segev and W. Rall. Computational study of an excitable dendritic spine. *J. Neurophysiol.*, 60:499–523, 1988.

[114] C. R. Shields, J. Klooster, Y. Claassen, M. Ul-Hussain, G. Zoidl, R. Dermietzel, and M. Kamermans. Retinal horizontal cell-specific promoter activity and protein expression of zebrafish Connexin 52.6 and Connexin 55.5. *J. Comp. Neurol.*, 501:765–779, 2007.

[115] R. G. Smith. Simulation of an anatomically defined local circuit: The cone-horizontal cell network in cat retina. *Vis. Neurosci.*, 12:545–561, 1995.

[116] R. G. Smith, M. A. Freed, and P. Sterling. Microcircuitry of the dark-adapted cat retina: functional architecture of the rod-cone network. *J. Neurosci.*, 6:3505–3517, 1986.

[117] D. C. Spray, Z.-C. Ye, and B. R. Ransom. Functional connexin "hemichannels": A critical appraisal. *Glia*, 54:758–773, 2006.

[118] R. H. Steinberg. The rod after-effect in S-potentials from the cat retina. *Vision Res.*, 9:1345–1355, 1969.

[119] R. H. Steinberg. Rod and cone contributions to S-potentials from the cat retina. *Vision Res.*, 9:1319–1329, 1969.

[120] R. H. Steinberg, M Reid, and P. L. Lacy. Distribution of rods and cones in retina of cat (*Felis Domesticus*). *J. Comp. Neurol.*, 148:229–248, 1973.

[121] W. K. Stell and D. O. Lightfood. Color-specific interconnections of cones and horizontal cells in the retina of the goldfish. *J. Comp. Neurol.*, 159:473–502, 1975.

[122] P. Sterling and J. B. Demb. In G. M. Shepherd, editor, *The synaptic organization of the brain*, chapter Retina, pages 217–270. Oxford University Press, New York, 2004.

[123] J. M. Sullivan and E. M. Lasater. Sustained and transient calcium currents in horizontal cells of the white bass retina. *J. Gen. Physiol.*, 99:85–107, 1992.

[124] M. Tachibana and A. Kaneko. gamma-aminobutyric acid acts at axon terminals of turtle photoreceptors: difference in sensitivity among cell types. *Proc. Natl. Acad. Sci. USA*, 81:7961–7964, 1984.

[125] T. Tatsukawa, H. Hirasawa, A. Kaneko, and M. Kaneda. GABA-mediated component in the feedback response of turtle retinal cones. *Vis. Neurosci.*, 22:317–324, 2005.

[126] W. B. Thoreson and D. A. Burkhardt. Effects of synaptic blocking agents on the depolarizing responses of turtle cones evoked by surround illumination. *Vis. Neurosci.*, 5:571–583, 1990.

[127] W. B. Thoreson and D. A. Burkhardt. Ionic influences on the prolonged depolarization of turtle cones *in situ*. *J. Neurophysiol.*, 65:96–110, 1991.

[128] W. B. Thoreson, R. Katalin, E. Townes-Anderson, and R. Heidelberger. A highly Ca^{2+}-sensitive pool of vesicles contributes to linearity at the rod photoreceptor ribbon synapse. *Neuron*, 42:595–605, 2004.

[129] J.-I. Toyoda and M. Fujimoto. Analysis of neural mechanisms mediating the effect of horizontal cell polarization. *Vision Res.*, 23:1143–1150, 1983.

[130] Y. Ueda, A. Kaneko, and M. Kaneda. Voltage-dependent ionic currents in solitary horizontal cells isolated from cat retina. *J. Neurophysiol.*, 68:1143–1150, 1992.

[131] M. VanLeeuwen, I. Fahrenfort, T. Sjoerdsma, R. Numan, and M. Kamermans. Lateral gain control in the outer retina leads to potentiation of center responses of retinal neurons. *J. Neurosci.*, 29:6358–6366, 2009.

[132] N. Vardi, D. L. Kaufman, and P. Sterling. Horizontal cells in cat and monkey retina express different isoforms of glutamic-acid decarboxylase. *Vis. Neurosci.*, 11:135–142, 1994.

[133] N. Vardi, P. Masarachia, and P. Sterling. Immunoreactivity to GABA(A) receptor in the outer plexiform layer of the cat retina. *J. Comp. Neurol.*, 320:394–397, 1992.

[134] J. Verweij, E. P. Hornstein, and J. L. Schnapf. Surround antagonism in macaque cone photoreceptors. *J. Neurosci.*, 23:10249–10257, 2003.

[135] J. Verweij, M. Kamermans, and H. Spekreijse. Horizontal cells feed back to cones by shifting the cones calcium-current activation range. *Vision Res.*, 36:3943–3953, 1996.

[136] J. Verweij, M. Kamermans, E. C. van Den Aker, and H. Spekreijse. Modulation of horizontal cell receptive fields in the light adapted goldfish retina. *Vision Res.*, 36:3913–3923, 1996.

[137] J. P. Vessey, M. R. Lalonde, H. A. Mizan, N. C. Welch, M. E. M. Kelly, and S. Barnes. Carbenoxolone inhibition of voltage-gated Ca channels and synaptic transmission in the retina. *J. Neurophysiol.*, 92:1252–1256, 2004.

[138] J. P. Vessey, A. K. Stratis, B. A. Daniels, N. D. Silva, M. G. Jonz, M. R. Lalonde, W. H. Baldridge, and S. Barnes. Proton-mediated feedback inhibition of presynaptic calcium channels at the cone photoreceptor synapse. *J. Neurosci.*, 25:4108–4117, 2005.

[139] J. Vigh and P. Witkovsky. Sub-millimolar cobalt selectively inhibits the receptive field surround of retinal neurons. *Vis. Neurosci.*, 16:159–168, 1999.

[140] X.-J. Wang and J. Rinzel. Alternating and synchronous rhythms in reciprocally inhibitory model neurons. *Neural Comput.*, 4:84–97, 1992.

[141] X.-J. Wang, J. Rinzel, and M. A. Rogawski. A model of the T-type calcium current and the low-threshold spikes in thalamic neurons. *J. Neurophysiol.*, 66:839–850, 1991.

[142] F. S. Werblin and J. E. Dowling. Organization of the retina of the mudpuppy, *Necturus Maculosus*. II. intracellular recording. *J. Neurophysiol.*, 32:339–355, 1969.

[143] R. W. Williams, C. Cavada, and F. Reinososuarez. Rapid evolution of the visual system: A cellular assay of the retina and dorsal lateral geniculate nucleus of the spanish wildcat and the domestic cat. *J. Neurosci.*, 13:208–228, 1993.

[144] P. Witkovsky, Y. Schmitz, A. Akopian, D. Krizaj, and D. Tranchina. Gain of rod to horizontal cell synaptic transfer: relation to glutamate release and a dihydropyridine-sensitive calcium current. *J. Neurosci.*, 17:7297–7306, 1997.

[145] S. M. Wu. Input-output relations of the feedback synapse between horizontal cells and cones in the tiger salamander retina. *J. Neurophysiol.*, 65:1197–1206, 1991.

[146] S. M. Wu. Synaptic transmission in the outer retina. *Annu. Rev. Physiol.*, 56:141–168, 1994.

[147] T. Yagi and P. R. MacLeish. Ionic conductances of monkey solitary cone inner segments. *J. Neurophysiol.*, 71:656–665, 1994.

[148] F. Yamamoto, G. A. Borgula, and R. H. Steinberg. Effects of light and darkness on pH outside rod photoreceptors in the cat retina. *Exp. Eye Res.*, 54:685–697, 1992.

[149] K. W. Yau. Phototransduction mechanisms in retinal rods and cones. *Invest. Ophthalmol. Vis. Sci.*, 35:9–32, 1994.

[150] S. Yazulla and J. Kleinschmidt. Carrier-mediated release of GABA from retinal horizontal cells. *Brain Res.*, 263:63–75, 1983.

[151] S. Yazulla, K. M. Studholme, J. Vitorica, and A. L. De Blas. Immunocytochemical localization of GABA(A) receptors in goldfish and chicken retinas. *J. Comp. Neurol.*, 280:15–26, 1989.

[152] D. Zela. *A continuum spine model for the horizontal cell-to-cone feedback in cat outer retina*. PhD thesis, Arizona State University, 2001.

[153] J. Zhang and S. M. Wu. Connexin 35/36 gap junction proteins are expressed in photoreceptors of the tiger salamander retina. *J. Comp. Neurol.*, 470:1–12, 2004.